

THERMAL STRESS ANALYSIS OF FUEL ELEMENT IN PARTICLE BED REACTOR

by

Lu Han

B.S. in Engineering, Huazhong University of Science and Technology, 2010

Submitted to the Graduate Faculty of
Swanson School of Engineering in partial fulfillment
of the requirements for the degree of
Master of Science in Mechanical Engineering

University of Pittsburgh

2013

UNIVERSITY OF PITTSBURGH
SWANSON SCHOOL OF ENGINEERING

This thesis was presented

by

Lu Han

It was defended on

July 18, 2013

and approved by

Dr. William S. Slaughter, Ph.D., Associate Professor, Department of Mechanical Engineering
and Material Science

Dr. Anne M. Robertson, Ph.D., Professor, Department of Mechanical Engineering

Dr. Patrick Smolinski, Ph.D., Associate Professor, Department of Mechanical Engineering
and Material Science

Thesis Advisor: Dr. William S. Slaughter, Ph.D., Associate Professor, Department of
Mechanical Engineering and Material Science

Copyright © by Lu Han

2013

**THERMAL STRESS ANALYSIS OF FUEL ELEMENT IN PARTICLE BED
REACTOR**

Lu Han, M.S.

University of Pittsburgh, 2013

In this paper, a method of determination of temperature and thermal stress distributions in a fuel element of a new gas-cooled, thermal spectrum particle bed reactor (GCT-PBR) was derived. It was capable of predicting failure and giving feedback on dimension design. To describe the fuel element, a three-layer conductive porous cylinder with infinite height and different materials was considered. A linear model of heat transfer in a one-dimensional porous medium with uniform internal energy source in cylindrical coordinate was first developed. Only steady state was considered. In thermal stress analysis, the thermal and mechanical properties of the solid phase and coolant were taken as constants, which were independent of temperature and time. Failure analysis was conducted based on von Mises criteria. The effect of geometry on thermal stress was investigated. It was shown that hot frit experienced the highest thermal stress and within design requirement, a thinner hot frit and a thicker cold frit would give a better performance.

TABLE OF CONTENTS

PREFACE.....	X
1.0 INTRODUCTION	1
1.1 SUMMARY.....	1
1.2 PROBLEM STATEMENT	2
2.0 BACKGROUND.....	5
2.1 OVERVIEW	5
2.2 GCT-PBR DESCRIPTION	7
2.2.1 Reactor structure.....	7
2.2.2 Fuel element design	10
2.3 MODEL.....	13
3.0 HEAT TRANSFER IN PARTICLE BED.....	18
3.1 FORMULATION OF THE PROBLEM.....	18
3.2 ASSUMPTIONS MADE IN THE DERIVATION OF ENERGY EQUATION.....	19
3.3 ENERGY EQUATION FOR PARTICLE BED.....	20
3.4 AUXILIARY CONDITIONS	23
4.0 THERMAL STRESS ANALYSIS OF FUEL ELEMENT.....	25
4.1 SUMMARY.....	25
4.2 ASSUMPTIONS MADE IN THERMAL STRESS ANALYSIS.....	26
4.3 GOVERNING EQUATIONS FOR PLANE STRAIN PROBLEM.....	26

4.4	AUXILIARY CONDITIONS	28
4.4.1	Boundary conditions.....	28
4.4.2	Initial conditions	29
4.4.3	Continuity conditions	29
5.0	SOLUTIONS AND DISCUSSIONS	34
5.1	SOLUTION TO ENERGY EQUATION	34
5.2	OUTLINE TO SOLVE DISPLACEMENT AND THERMAL STRESS EQUATIONS	35
5.3	RESULTS AND DISCUSSIONS.....	37
5.3.1	Temperature distribution	37
5.3.2	Displacement and thermal stress analysis	40
5.3.3	Geometry and thermal stresses	45
6.0	CONCLUSIONS.....	50
	BIBLIOGRAPHY	52

LIST OF TABLES

Table 2.1 Mechanical and thermal properties of SiC	15
Table 2.2 Mechanical and thermal properties of the particle bed and its dimension.....	16
Table 2.3 Properties of helium and some other useful parameters	17

LIST OF FIGURES

Figure 2.1 Outline of a typical reactor assembly [19].	8
Figure 2.2 Reactor cross-section [20].	9
Figure 2.3 Particle Bed Reactor Based Rocket Engine [13].	10
Figure 2.4 Axial view of the fuel element with coolant flow paths [2]	12
Figure 2.5 Cross-section of the fuel element [2].	13
Figure 2.6 Analytical model of the fuel element in cylindrical coordinate	14
Figure 3.1 Analytical model of the particle bed, cylindrical geometry	19
Figure 3.2 Typical control element at r of thickness dr , radian $d\theta$ and unit height from the particle bed.	21
Figure 4.1 Pressure in the inner cylinder with inner radius r_1 and outer radius r_2	30
Figure 4.2 Pressure in the middle cylinder with inner radius r_2 and outer radius r_3	31
Figure 4.3 Pressure in the outer cylinder with inner radius r_3 and outer radius r_4	32
Figure 5.1 Temperature distributions in the middle cylinder with mass flow rate of 0.4, 0.6, and 0.8 $\text{kg}\cdot\text{s}^{-1}\cdot\text{m}^{-1}$, respectively.	38
Figure 5.2 Temperature distribution in the middle cylinder with mass flow rate of 0.5 $\text{kg}\cdot\text{s}^{-1}\cdot\text{m}^{-1}$ and outlet temperature of 1000 °C.	39
Figure 5.3 Displacement distribution in the three-layer cylinder with $r_1=0.0406$ m, $r_4=0.0566$ m.	40
Figure 5.4 Radial thermal stress in the three-layer cylinder with $r_1=0.0406$ m, $r_4=0.0566$ m.	41
Figure 5.5 Circumferential stress in the three-layer cylinder with $r_1=0.0406$ m, $r_4=0.0566$ m.	42

Figure 5.6 Axial stress in the three-layer cylinder with $r_1=0.0406$ m, $r_4=0.0566$ m.	43
Figure 5.7 Von Mises stress in the three-layer cylinder with $r_1=0.0406$ m, $r_4=0.0566$ m.....	44
Figure 5.8 Radial thermal stresses in the three-layer cylinder with hot frit of 3mm ($r_1=0.0406$ m), 5mm ($r_1=0.0386$ m), and 7mm ($r_1=0.0366$ m), respectively.	45
Figure 5.9 Circumferential thermal stresses in the three-layer cylinder with hot frit of 3mm ($r_1=0.0406$ m), 5mm ($r_1=0.0386$ m), and 7mm ($r_1=0.0366$ m), respectively.	46
Figure 5.10 Radial thermal stresses in the three-layer cylinder with cold frit of 3mm ($r_4=0.0566$ m), 5mm ($r_4=0.0586$ m), and 7mm ($r_4=0.0606$ m), respectively.	47
Figure 5.11 Circumferential thermal stresses in the three-layer cylinder with cold frit of 3mm ($r_4=0.0566$ m), 5mm ($r_4=0.0586$ m), and 7mm ($r_4=0.0606$ m), respectively.	48

PREFACE

I would like to express my appreciation to all those who helped me in so many ways. A special thanks goes to my advisor, Dr. William S. Slaughter, who gave me the opportunity to work with him on this subject and helped me so much throughout the entire project. Also I would like to thank Dr. Anne M. Robertson and Dr. Patrick Smolinski for serving on the committee and providing so many valuable suggestions. Finally, and most importantly, thank you to my family, boyfriend and friends who understand me and support me all the way.

1.0 INTRODUCTION

1.1 SUMMARY

A Particle Bed Reactor (PBR) is a gas-cooled, solid-core nuclear reactor by which energy is produced by nuclear fission and is removed by gas coolant. Unlike other reactors, the PBR makes nuclear fuel into small, coated particulate spheres and packs them between two concentric cylindrical shells [1]. The two cylindrical shells are called frits and the retention between them is called particle bed. The frits are porous to allow the flow of coolant but strong enough to confine the fuel particles. For the spherical fuel particles give a high surface area and are direct cooled by gas coolant, this design increases heat transfer efficiency and outlet propellant temperature of nuclear reactor. With distinct advantages of compactness, great energy efficiency and high power density, the PBR is an excellent choice for space use and nuclear thermal propulsion application.

The particle bed reactor concept was originally proposed by researchers at Brookhaven National Thermal Program (BNL) in the early 1980's. Most of the PBR development was done as part of the U.S. Air Force Space Nuclear Thermal Propulsion program (SNTP) which lasted until 1993 [1]. The SNTP program aimed at designing a hydrogen-cooled PBR with an outlet temperature of 3000K for various U.S. Air Force missions and ended with great achievements. It verified feasibility of the PBR, developed fuel particles which could operate at very high

temperature, demonstrated a prototypical PBR engine, and figured out key points in thermal-hydraulics and structural performance of PBR.

The PBR concept talked here is a new gas-cooled, thermal spectrum particle bed reactor (GCT-PBR) proposed by Dr. Metzger John of University of Pittsburgh in 2012. Unlike the one designed for SNTP, the GCT-PBR will operate at modest temperature with an anticipated exit gas temperature of 650-1000 °C [2]. The GCT-PBR has the ability to remove ~1MW/liter from the particle bed using helium as coolant and will operate for a long time between shut down. It has the potential to improve energy efficiency, save cost, be friendly to environment, and move nuclear reactor technology forward. The GCT-PBR will have various performances in space and terrestrial applications.

The main objective of this thesis was to study heat transfer and thermal stresses of a fuel element in the reactor. The fuel element is the basic building block of the Particle Bed Reactor. It is the place where nuclear reaction, heat transfer, and heat removal take place. The fuel element experiences high temperature in high pressure with coolant flowing through. Heat transfer between the flowing coolant and still particle bed will induce a high temperature gradient which will cause thermal stresses. The thermal stresses can be large enough to force failure in materials. To be able to predict these failures and give feedback on the structure design, a comprehensive understanding of the temperature distribution and resulting thermal stress is essential.

1.2 PROBLEM STATEMENT

The outlet temperature of GCT-PBR (650-1000 °C) is lower than the one designed for SNTP (~1649 °C), however, the temperature gradient can be steep for the distance of heat transfer is

very short (~1cm). This temperature gradient will set up high thermal stresses. If the thermal stresses exceed the strength limitation of the structural materials, crushing will happen and integrity of structure will be destroyed. Thus to figure out temperature and thermal stress distributions is very important in designing shape, selecting materials and deciding control parameters.

In this paper, a method of determining temperature and thermal stress distributions in a three-layer cylinder with different materials which represents the fuel element will be derived. Only steady state is considered here. In the process of heat transfer, the temperatures of the fluid phase and solid phase are taken the same. In thermal stress analysis, only thermal stresses generated by temperature gradient induced by heat transfer between the flowing coolant and still particle bed is taken into consideration. The thermal and mechanical properties of the solid phase and coolant are taken as constants, which do not change with temperature or time.

The problem to be investigated here encompasses the following objectives:

1. The description of heat transfer process in the particle bed in cylindrical coordinate. The energy equation governing the mechanism of heat transfer in the particle bed with a uniform energy source is formulated.
2. The solution to the energy equation. Several numerical solutions are displayed and the factors which influence the temperature distribution are studied.
3. Displacement and thermal stress analyses in the fuel element, which is composed of a cold frit, a particle bed and a hot frit, based on the obtained temperature profile. Failure analysis is also conducted by von Mises criteria.
4. The study of fuel element geometry and thermal stress distribution. How changing dimension of fuel element affects thermal stress is investigated, which includes how

changing the cold and hot frit thicknesses affect thermal stress distributions in r -direction and θ -direction.

2.0 BACKGROUND

2.1 OVERVIEW

The idea of using nuclear energy for space propulsion is not new. Going back a century ago, R. Goddard conceived using radium as an energy source in 1906 and Robert Esnault-Pelterie pointed nuclear energy was indispensable for space travel in 1912 [1]. Over the years, a number of books and articles [3-7] have been published on this subject.

In the early years of space exploration and propulsion system design, the former Soviet Union and the United States were the two leading countries. The U.S. government put attention on this area long time ago. In the history of United States, space based reactor design has been evolving since the ROVER program of 1960s and its subsidiary NERVA program [8], In the NERVA program, Nuclear Thermal Propulsion technology base was established and a propulsion system was developed, modified and tested [9, 10]. Though much was gained from the two programs, there were three big problems that limited the nuclear rocket performance in the earlier designs: big size, low power density, and high pressure drop.

To overcome these problems, a fundamental change in the conceptual nuclear reactor was essential. For sphere has the largest area per unit volume of all common shapes and fuel elements composed of randomly packed spheres can minimize the pressure drop, the idea of packing spherical fuel particulates to form fuel elements emerged. The first design using this concept was

the Rotating Bed Reactor (RBP) [11, 12] which had a rotating porous outlet frit. The particles were packed on the wall by centrifugation and there was no requirement for inner frit. This concept was investigated for about 10 years until the national Nuclear Thermal Propulsion effort was stopped.

After a lull in the early 1980s, United States' interest in this area has been rejuvenated. In 1982, a study of fixed bed reactor (FBR) started [13]. There was no rotating component in the FBR which was an advantage over RBP. However, the FBR had several disadvantages which limited its performance, such as thick particle-fuel bed, low economic efficiency and stringent requirements for hot frit material. Things started to change in 1985 when a novel concept was proposed [14] by Dr. James Powell of Brookhaven National Thermal Program (BNL), called Particle Bed Reactor (PBR).

The PBR packed a number of fuel particles within two concentric, cylindrical, porous frits to form a fuel element. Several fuel elements with moderator, control rods, and other components would be assembled to form a reactor. Coolant would pass radially through the fuel elements and leave the reactor through nozzle to remove generated heat. With unique characteristics of compact size, high power density, and low weight, this concept was pursued with interest [15-18] the time it was proposed.

Most work of PBR was done in Space Nuclear Application Program (SNTP) [19] which started in 1987 and was funded by the Strategic Defense Initiative (SDI) and the U. S. Air Force. The SNTP Program aimed at providing the nation a new, high performing hydrogen-cooled PBR with an outlet temperature of 3000K. In the program, the feasibility of the PBR was verified and a ground demonstration of a prototypical PBR engine was performed. The program lasted for

more than 10 years and identified major technical issues in fuel, material and thermal-hydraulic areas, which were necessary to develop the rocket engine based on a PBR.

The PBR for SNTP program had an extremely high outlet temperature and the requirements for material and operation were stringent. Now it is time to design varied PBR depending on different applications. In 2012, Dr. Metzger John in University of Pittsburgh proposed a new concept of a gas-cooled, thermal spectrum particle bed reactor (GCT-PBR) based the PBR designed for SNTP. Differently, the GCT-PBR will operate for longer period and work at modest temperature. With the technology developments and successes of the SNTP Program, the GCT-PBR has a strong foundation to start from.

2.2 GCT-PBR DESCRIPTION

2.2.1 Reactor structure

The basic components of the GCT-PBR are fuel elements array, moderator, control rods, and reflector. The fundamental fuel element design contains two frits and a fuel particle bed located just between them. Each fuel element is arranged in a hexagonal lattice, and is surrounded by light water which serves as the moderator. Several hexagonal patterns are assembled to form a core. The reflector is just located outside the core. Figure 2.1 depicts an outline of a typical reactor assembly and Figure 2.2 illustrates a schematic structure of a reactor core in cross section. The reflector is used to scatter neutrons to prevent them leaking from the core. The moderator serves to slow down the neutrons released during fission to maintain a chain reaction and the control rods are to control the speed of the fission reaction by absorbing neutrons. The

reactor, combined with other main structures such as propellant tank, thrust structure, pressure vessel, and nozzle, forms a thermal rocket engine, see Figure 2.3.

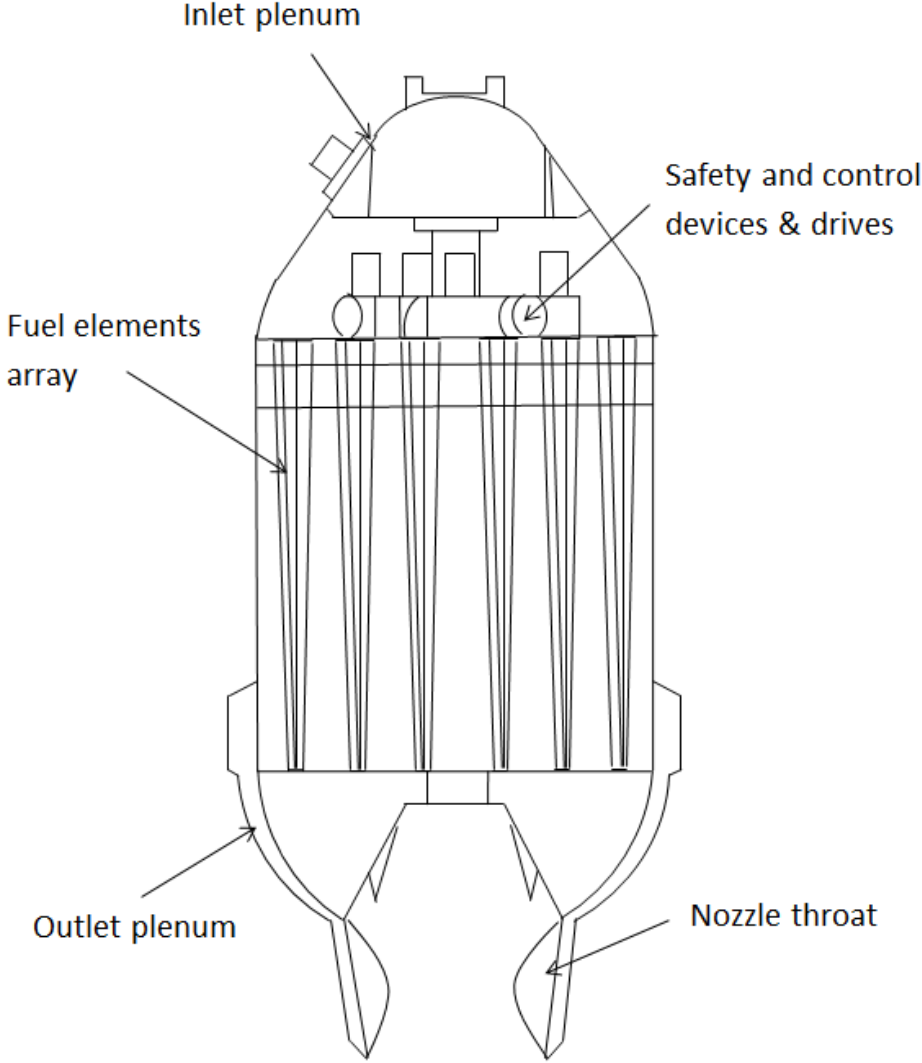


Figure 2.1 Outline of a typical reactor assembly [19].

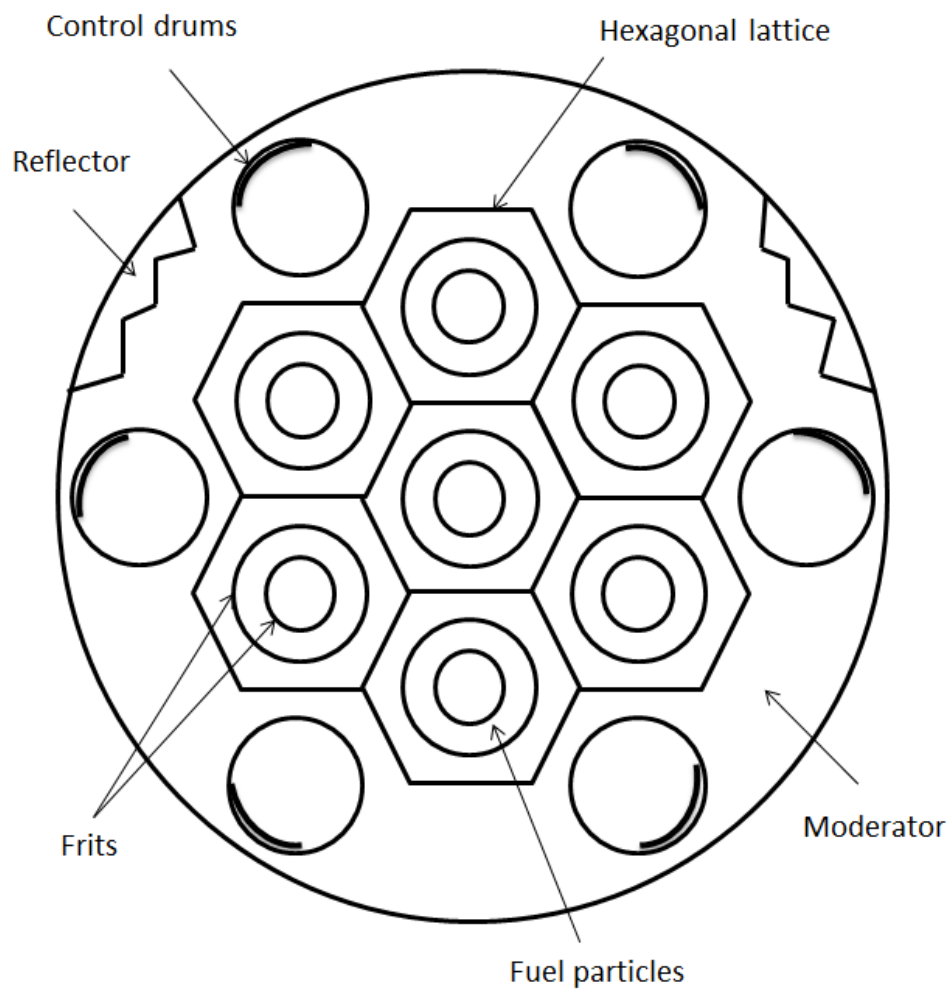


Figure 2.2 Reactor cross-section [20].

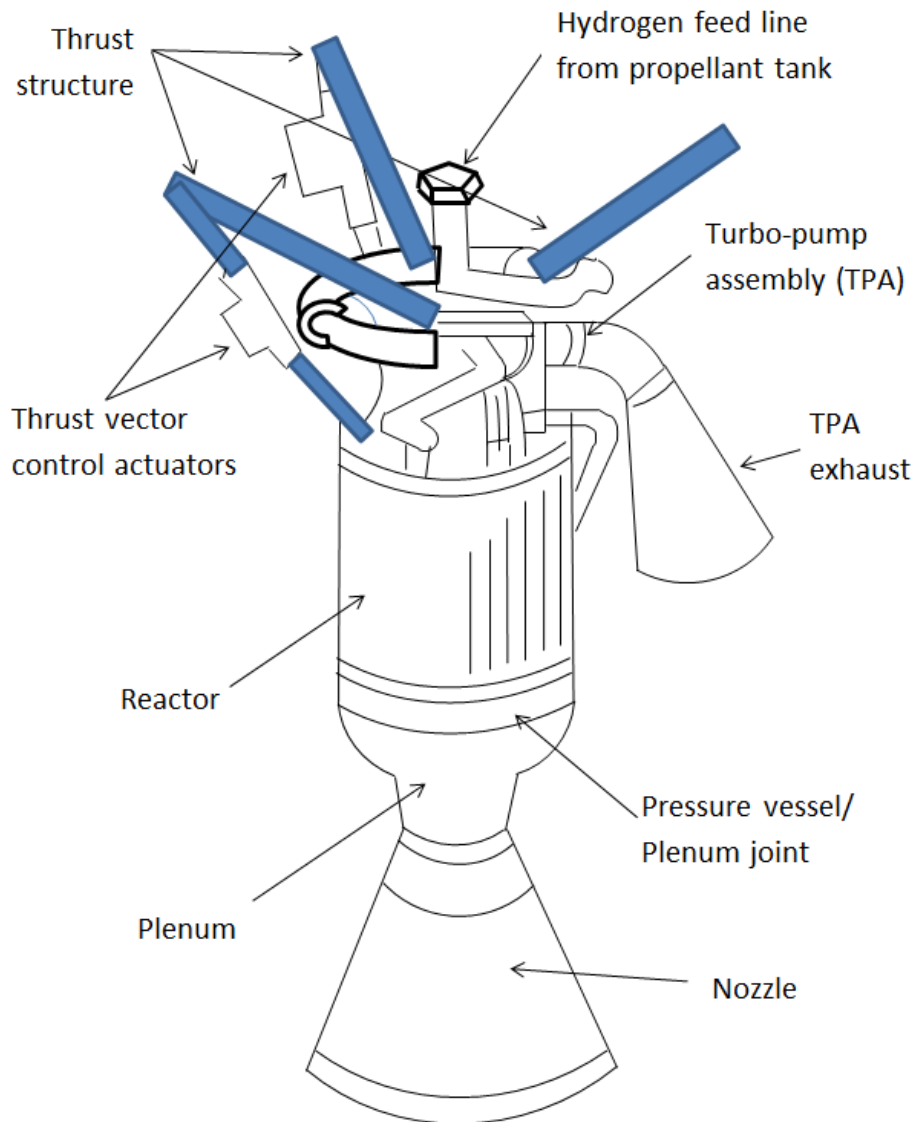


Figure 2.3 Particle Bed Reactor Based Rocket Engine [13].

2.2.2 Fuel element design

Each fuel element of the GCT-PBR consists of a fuel particle bed located in two coaxially cylindrical shells, called frits. The spherical fuel particles are randomly packed in the particle bed. The outer frit, called cold frit, is an outer tapered cylindrical shell enclosing the fuel particle

bed; while the inner frit, called hot frit, is the inner cylindrical shell through which heated coolant gas will pass through to the centered outlet channel. Both frits are made of porous material. They will control and meter the coolant flow axially and circumferentially. During operation, the preheated cold gas goes axially through the inlet plenum, then traverses in a radial direction through the cold (outer) frit, particle bed, and hot (inner) frit, and finally goes out axially through the outlet plenum, as is shown in Figure 2.4 and Figure 2.5.

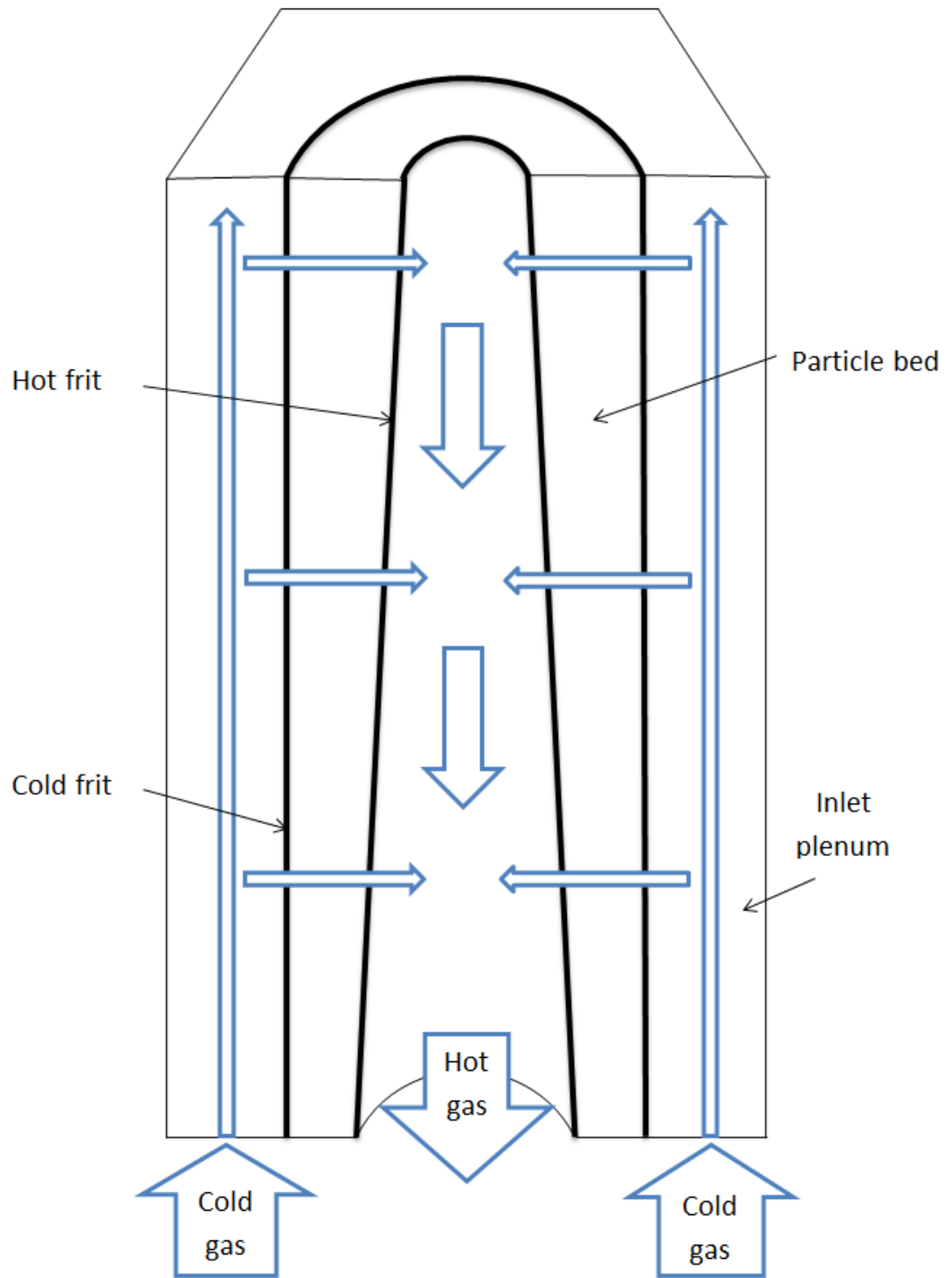


Figure 2.4 Axial view of the fuel element with coolant flow paths [2]

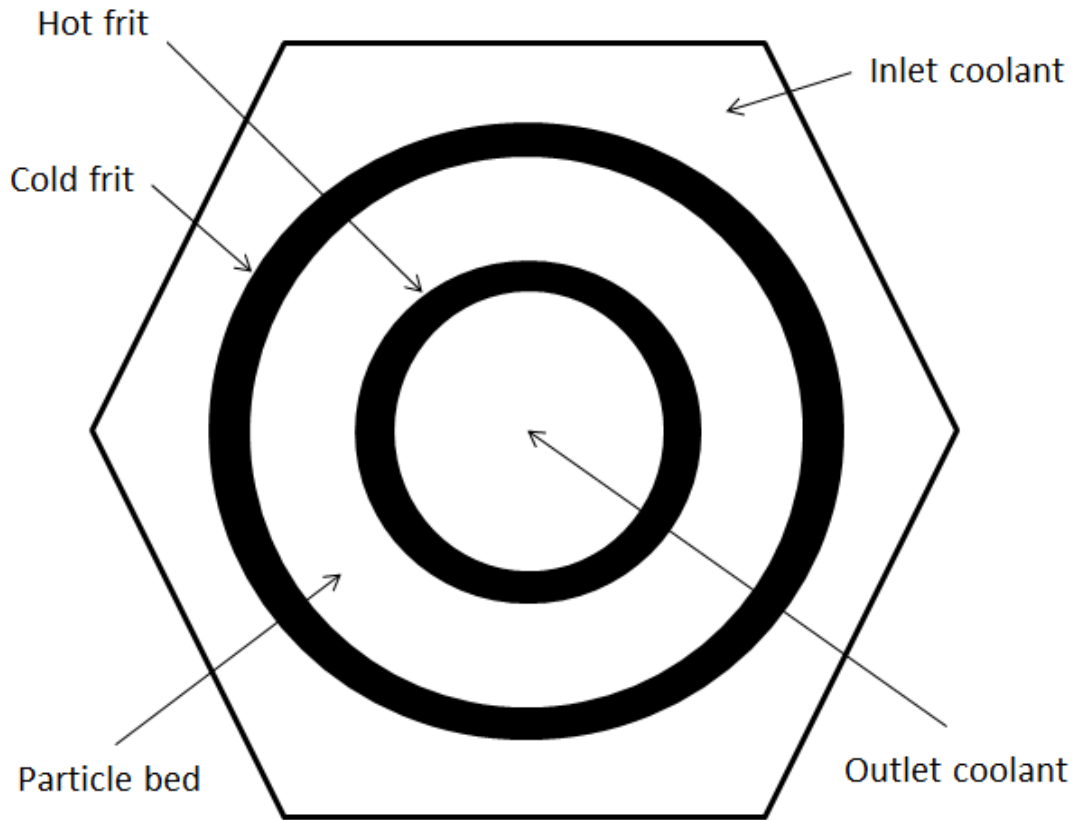


Figure 2.5 Cross-section of the fuel element [2].

2.3 MODEL

To describe the fuel element, a three-layer porous cylinder with infinite height and different materials was considered, see Figure 2.6. The inner cylinder with radii r_1 and r_2 represents the cold frit. The middle cylinder with radii r_2 and r_3 represents the particle bed. The outer cylinder with radii r_3 and r_4 represents the cold frit. The inner and outer cylinders are made of the same material (material 1) and the middle cylinder is made of a different material (material 2). All

cylinders are porous. Heat transfer process was only considered in the middle cylinder. The temperatures of the inner and outer frits were assumed to be constants. Thermal stress analysis was taken in the three cylinders based on established temperature distribution.

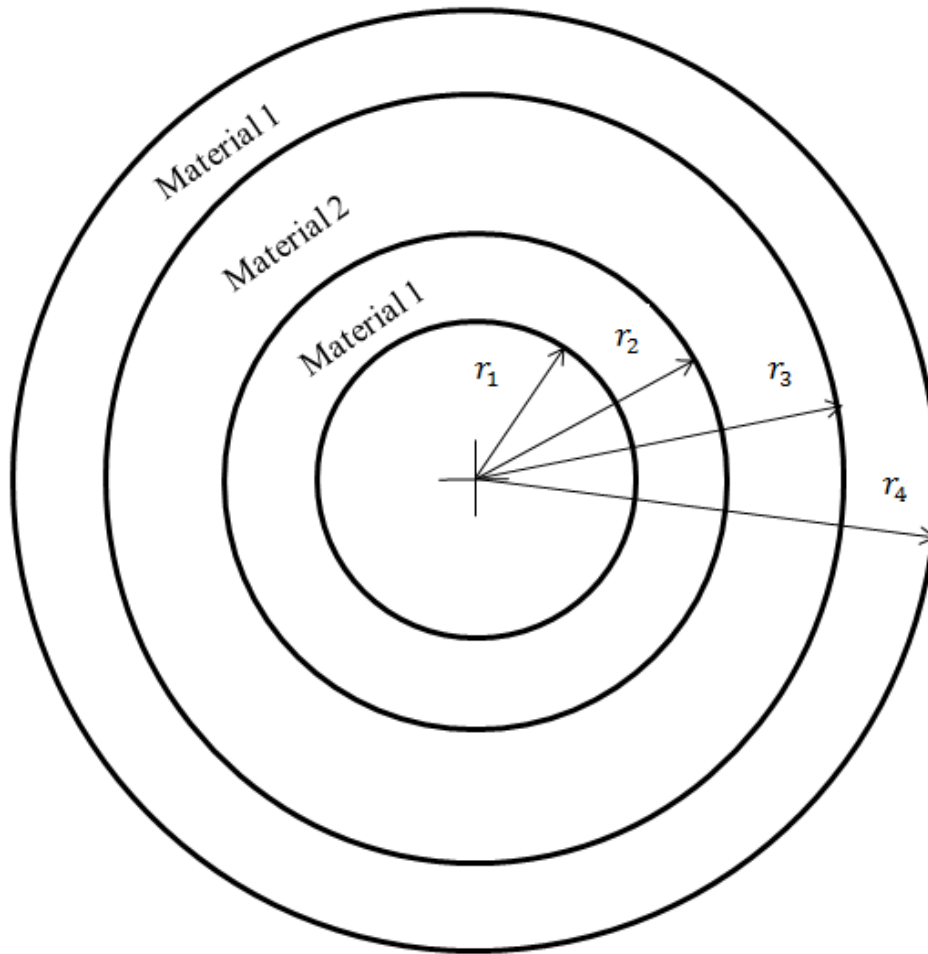


Figure 2.6 Analytical model of the fuel element in cylindrical coordinate

Both cold frit and hot frit are made of Silicon Carbide (*SiC*). The mechanical and thermal properties of *SiC* are listed in Table 2.1. It is assumed the fuel particles are randomly packed between the frits with packing density of 64%. The dimension and properties of the particle bed

are presented in Table 2.2. Helium is chosen as coolant with its properties and other useful parameters listed in Table 2.3. The thickness of the cold frit and hot frit are expected to be on the order of 3~7 mm.

Table 2.1 Mechanical and thermal properties of SiC

Property	Value
Thermal conductivity	60 W/(m·°C)
Coefficient of thermal expansion	$4.9 \times 10^{-6}/^{\circ}\text{C}$
Elastic modulus	410 GPa
Poisson's ratio	0.14
Compressive strength	390 MPa
Maximum use temperature (no load)	1650°C
Flexural strength	550 MPa

Table 2.2 Mechanical and thermal properties of the particle bed and its dimension

Property	Value
Porosity	64%
Thermal conductivity	38.4 W/(m· °C)
Coefficient of thermal expansion	4.9*10 ⁻⁶ /°C
Elastic modulus	262.4 GPa
Poisson's ratio	0.0896
Energy strength	1*10 ⁹ W
Inner radius of the particle bed (r_2)	0.0436 m
Outer radius of the particle bed (r_3)	0.0536 m

Table 2.3 Properties of helium and some other useful parameters

Items	Value
Specific heat of helium	5190 J/(kg·°C)
Thermal conductivity of helium	0.142 W/(m·°C)
Density of helium	0.1786 g/L
Inlet temperature	200°C
Outlet temperature	1000°C
Room temperature	25°C
Cold frit thickness	3~7 mm
Hot frit thickness	3~7 mm

3.0 HEAT TRANSFER IN PARTICLE BED

3.1 FORMULATION OF THE PROBLEM

The particle bed reactor is an energy exchange device which transfers nuclear energy into heat. To some extent, the performance of fuel and coolant in the core determines the reactor's service and economic value. To describe heat transfer process in the particle bed and provide information to prevent temperature from exceeding design limits, a model of fluid flowing through porous medium was taken here.

Many studies [21-25] have been conducted on theoretical analysis of heat transfer in porous medium. In this chapter, heat transfer in a one-dimensional porous medium with uniform internal heat source in cylindrical coordinate was considered. Based on the model talked in Chapter 2.3, the middle cylinder with inner radius r_2 and outer radius r_3 represented the particle bed, see Figure 3.1. The direction of flowing fluid was taken in the negative radial direction which was in accord with the movement of coolant in the particle bed. Energy equation governing the mechanism of heat transfer was formulated. The assumptions made in the derivation and the auxiliary conditions associated with the energy equation were also enumerated.

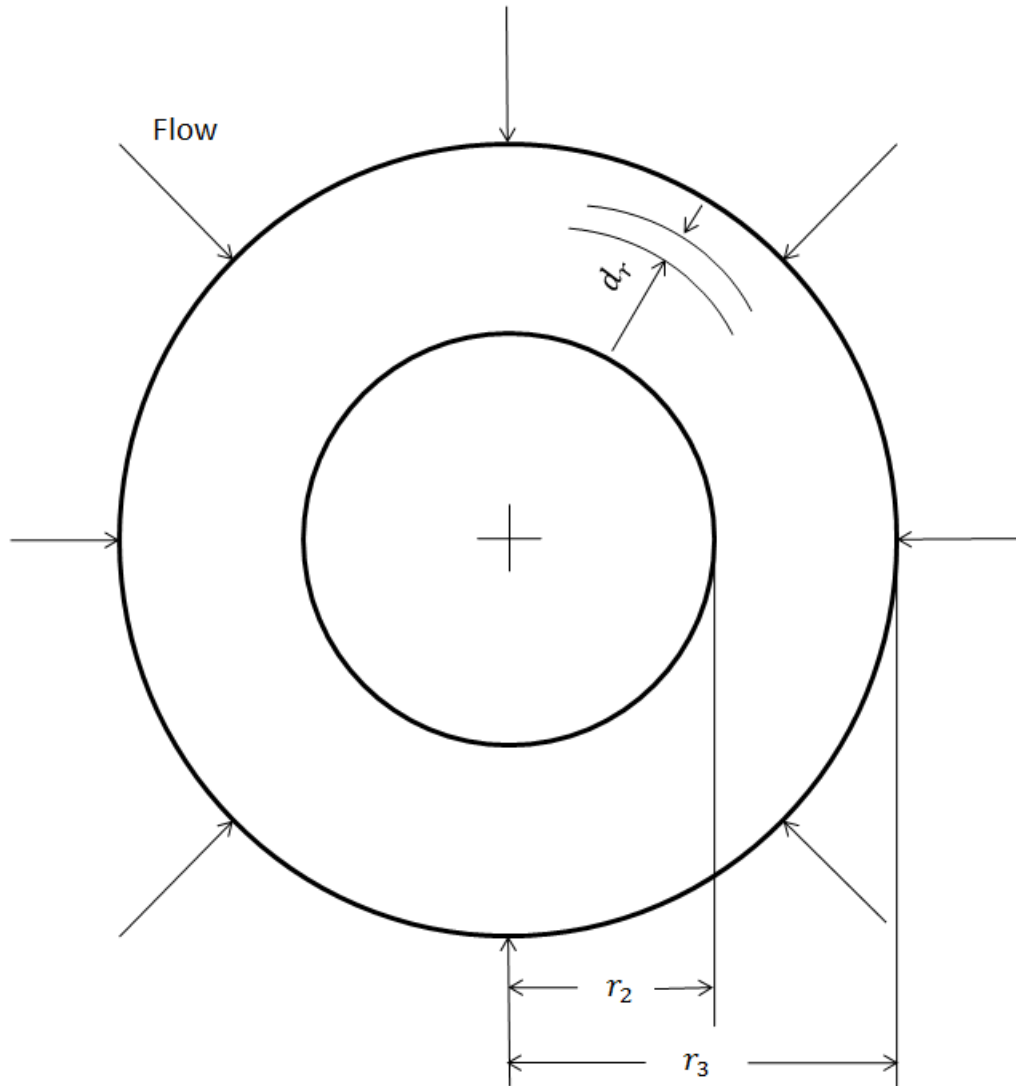


Figure 3.1 Analytical model of the particle bed, cylindrical geometry

3.2 ASSUMPTIONS MADE IN THE DERIVATION OF ENERGY EQUATION

To simplify the model and reduce calculation time, some assumptions are made in the formulation of energy equation, see below.

1. Only heat transfer in steady state is taken into consideration.

2. The heat flow is one-dimensional, that is, in r -direction only.
3. The temperatures of the gas phase and solid phase are equal.
4. The physical and thermal properties of the porous body and the fluid are constant.
5. Heat conduction in the fluid phase is neglected.
6. Heat transfer by radiation, which can occur at elevated temperature, is negligible here.

3.3 ENERGY EQUATION FOR PARTICLE BED

Based on the above assumptions, energy equation for the particle bed can be derived by applying the law of conservation of energy on an elemental control volume. For the model talked here, the law of conservation of energy can be stated as follows: In a control volume, the rate of thermal energy accumulated (\dot{E}_{ac}) is equal to the rate of thermal energy flows in (\dot{E}_{in}) plus the rate of thermal energy generated by nuclear fission (\dot{E}_{gen}) minus the rate of thermal energy flows out (\dot{E}_{out}). In equation form, it is,

$$\dot{E}_{ac} = \dot{E}_{in} + \dot{E}_{gen} - \dot{E}_{out} \quad (3.1)$$

Taking an infinite small element at r of thickness dr , radian $d\theta$, and unit height, called a control element, see Figure 3.2, the effort remained was to express each term in Equation (3.1) .

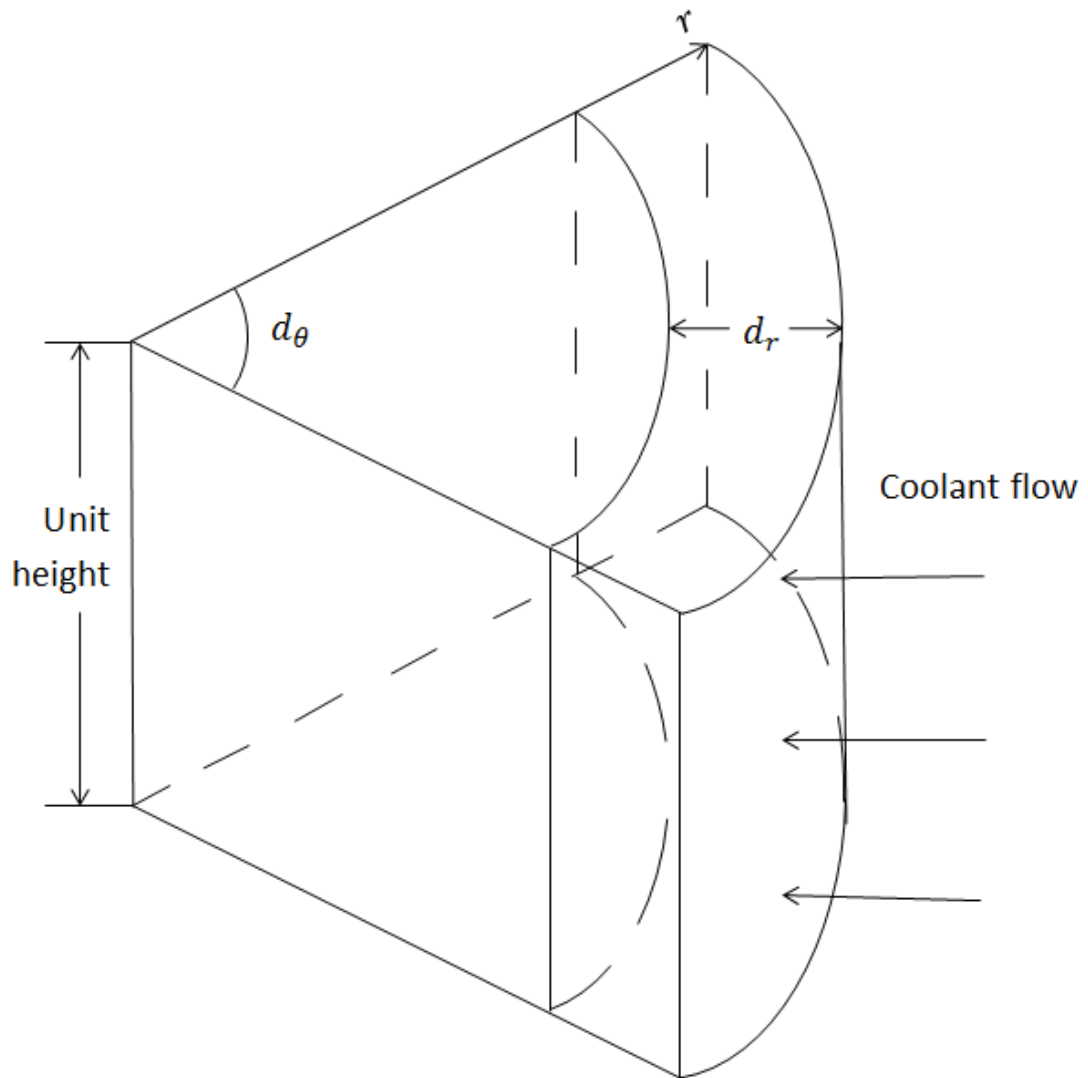


Figure 3.2 Typical control element at r of thickness dr , radian $d\theta$ and unit height from the particle bed

Since we assumed all the energy generated is removed by the coolant in steady state, the rate of thermal energy accumulated in the control element is zero, so

$$\dot{E}_{ac} = 0 \quad (3.2)$$

The rate of energy flows in can be written as the rate of energy conducted in and the rate of energy convected in. Applying Fourier's law [26], the rate of energy entered the control element by conduction can be expressed in terms of temperature gradient,

$$-k_s \frac{dT}{dr} (rd\theta \cdot 1) \quad (3.3)$$

And the rate of convective energy flows in can be written by increase of internal energy of the fluid,

$$\frac{\dot{m}C_{pf}}{2\pi r} (rd\theta \cdot 1)T \quad (3.4)$$

So the total energy entering the volume has the following form

$$\dot{E}_{in} = -k_s \frac{dT}{dr} (rd\theta \cdot 1) + \frac{\dot{m}C_{pf}}{2\pi r} (rd\theta \cdot 1)T \quad (3.5)$$

where

k_s is thermal conductivity of solid phase,

dT/dr is temperature gradient,

$(rd\theta \cdot 1)$ is the lateral surface of the element,

\dot{m} is mass flow rate per unit height,

C_{pf} is specific heat of the fluid phase.

If the rate of heat generation by nuclear fission per unit volume is \dot{q} , the rate of thermal energy generated in the element has the following expression,

$$\dot{E}_{gen} = \dot{q}(rd\theta \cdot dr \cdot 1) \quad (3.6)$$

where

$(rd\theta \cdot dr \cdot 1)$ is the volume of the control element.

The rate of energy left the control volume can be expressed by the energy entered in plus the change of it with respect to dr .

$$\dot{E}_{out} = \dot{E}_{in} - \left(\frac{d\dot{E}_{in}}{dr} \right) dr \quad (3.7)$$

Substituting each form into Equation (3.1) and neglecting second-order differentials, the energy equation can be obtained,

$$-k_s \left(\frac{d^2T}{dr^2} + \frac{1}{r} \frac{dT}{dr} \right) + \frac{\dot{m}C_{pf}}{2\pi r} \frac{dT}{dr} + \dot{q} = 0 \quad (3.8)$$

where

$-k_s[d^2T/dr^2 + (1/r)(dT/dr)]$ means the net rate of heat added by conduction. It is the transport of thermal energy from one volume element to the next by conduction in the solid phase. The thermal conductivity of fluid phase is neglected in assumption.

$(\dot{m}C_{pf}/2\pi r)(dT/dr)$ means the energy transport in r-direction due to bulk movement of the fluid. It is the net rate of energy transport by convection and has a deep connection with the physical and dynamic properties of the fluid.

\dot{q} is the rate of heat generation by nuclear fission per unit volume.

3.4 AUXILIARY CONDITIONS

The auxiliary conditions, which are essential to obtain numerical solution of the energy equation, will be postulated here. The coolant is preheated to T_1 before entering the fuel element. Since we assume the temperature doesn't change in the cold frit, the temperature of the coolant entering the fuel element particle bed can be taken as T_1 . After travelling through the particle bed, the coolant gets a temperature rise Δt and leaves with temperature T_2 . So

$$T = T_1, \quad \text{at } r = r_3. \quad (3.9)$$

$$T = T_1 + \Delta t = T_2, \quad \text{at } r = r_2. \quad (3.10)$$

However, at steady state, the heat generated within the bed is equal to the heat removed from the bed, which means,

$$\dot{q}\pi(r_3^2 - r_2^2) = \dot{m}C_{pf}(\Delta t) \quad (3.11)$$

4.0 THERMAL STRESS ANALYSIS OF FUEL ELEMENT

4.1 SUMMARY

During operation, the fuel element is subjected to the most extreme environment, like high power density, high temperature, and high temperature gradient, which will cause high thermal stress and even crack in the fuel element. It is important to understand thermal stress in the fuel element to make sure it works safely. The determination of thermal stress is also a crucial part in shape design of the fuel element. Numerous papers have been published on the subject of thermal stress analysis in cylindrical structure. J. R. Matthews [27] calculated thermal stresses within a finite heat generating cylinder over a range of length to diameter ratios. Richard A. et al [28] gave an exact solution for thermal displacement and stresses in a finite elastic cylinder based on known radial temperature distribution. Orcan [29] presented the solution of elastic-plastic cylinder with uniform internal heat generation and free ends. Z. Y. Lee et al. [30] analyzed transient thermal stresses under temperature change in multilayered hollow cylinder by Laplace transform and finite difference method.

In this chapter, displacement and thermal stress analyses were conducted in the three-layer cylinder with different materials, see Figure 2.5. Only thermal stress generated by temperature gradient induced by heat transfer between the flowing coolant and still particle bed was taken into consideration. The temperature of the particle bed was taken from the energy

equation obtained in Chapter 3.0 . In the cold and hot frits, temperatures were taken as constants. Displacement and thermal stress analyses were illustrated in the following part. The assumptions made in the derivation and the auxiliary conditions were also enumerated.

4.2 ASSUMPTIONS MADE IN THERMAL STRESS ANALYSIS

To simplify the model, we assume

1. The material of each layer is homogeneous and isotropic.
2. The mechanical and thermal properties of each layer are constant with respect to temperature and time.
3. The boundaries (r_1 and r_4) of the three-layer cylinder are traction-free.
4. No external forces are applied.
5. Radial dimension of the fuel element is very small compared to its height in z -direction.
6. The three-layer cylinder is undeformed and is in a stress-free state at room temperature.
7. Thermal stress produced by radiation is neglected.

4.3 GOVERNING EQUATIONS FOR PLANE STRAIN PROBLEM

The governing equations are a set of equations that describe the relationship of displacement, strain and stress fields. They contain strain-displacement equations, constitutive equations, and equilibrium equations. By applying governing equations with specific assumptions and auxiliary conditions, numerical solutions of a problem can be got.

Since the radial dimension of the fuel element is very small compared to its height, the problem is reduced to a plane strain problem where the displacement field is independent of z-direction. The laws and equations formulated for plane strain problem can be used here.

In the following part, u_i , E_{ij} , S_{ij} , $i, j = r, \theta, z$ represented the displacement fields, strain fields, and stress fields, respectively. In cylindrical coordinate, $u_z = 0$ in a state of plane strain, so the governing equations have the following expressions [31],

Strain–displacement equations for plane strain problem in cylindrical coordinate are

$$\begin{aligned} E_{rr} &= \frac{\partial u_r}{\partial r} \\ E_{\theta\theta} &= \frac{1}{r} \left(\frac{\partial u_\theta}{\partial \theta} + u_r \right) \\ E_{r\theta} &= \frac{1}{2} \left(\frac{1}{r} \frac{\partial u_r}{\partial \theta} + \frac{\partial u_\theta}{\partial r} - \frac{u_\theta}{r} \right) \end{aligned} \quad (4.1)$$

Constitutive equations for plane strain problem in cylindrical coordinate are

$$\begin{aligned} S_{rr} &= 2\mu E_{rr} + \lambda E_{kk} - (3\lambda + 2\mu)\alpha(\Delta T) \\ S_{\theta\theta} &= 2\mu E_{\theta\theta} + \lambda E_{kk} - (3\lambda + 2\mu)\alpha(\Delta T) \\ S_{r\theta} &= 2\mu E_{r\theta} \\ S_{zz} &= \lambda E_{kk} - (3\lambda + 2\mu)\alpha(\Delta T) \end{aligned} \quad (4.2)$$

Equilibrium equations for plane strain problem in cylindrical coordinate are

$$\begin{aligned} \frac{\partial S_{rr}}{\partial r} + \frac{1}{r} \frac{\partial S_{r\theta}}{\partial \theta} + \frac{1}{r} (S_{rr} - S_{\theta\theta}) &= 0 \\ \frac{\partial S_{\theta r}}{\partial r} + \frac{1}{r} \frac{\partial S_{\theta\theta}}{\partial \theta} + \frac{2}{r} S_{\theta r} &= 0 \end{aligned} \quad (4.3)$$

where

$$E_{kk} = E_{rr} + E_{\theta\theta} \quad (4.4)$$

δ_{ij} is Kronecker delta, it is an indicial notation symbol defined as

$$\delta_{ij} \equiv \begin{cases} 1, & \text{if } i = j \\ 0, & \text{if } i \neq j \end{cases} . \quad (4.5)$$

α is thermal expansion coefficient,

ΔT is the temperature difference,

λ and μ are material parameters, known as the Lamé constant, which have the following expressions

$$\lambda = \frac{Y\nu}{(1+\nu)(1-2\nu)},$$

$$\mu = \frac{Y}{2(1+\nu)}. \quad (4.6)$$

ν is poisson's ratio,

Y is Young's modulus.

4.4 AUXILIARY CONDITIONS

The auxiliary conditions are composed of boundary conditions and continuous conditions. Applying the auxiliary conditions to the governing equations postulated earlier, the stress equation for each layer can be obtained.

4.4.1 Boundary conditions

The lateral surfaces of the three-layer cylinder are traction-free. From traction-stress equation [31], it can be seen that,

For the portion at $r = r_1$, the unit outward normal is $\mathbf{n} = -\mathbf{e}_r$ and the specified traction is $\mathbf{t} = 0$. It follows that

$$S_{rr}^{in} = 0, \quad S_{\theta r}^{in} = 0, \quad \text{when } r = r_1 \quad (4.7)$$

For the portion at $r = r_4$, the unit outward normal is $\mathbf{n} = \mathbf{e}_r$ and the specified traction is $\mathbf{t} = 0$. It follows that

$$S_{rr}^{out} = 0, \quad S_{\theta r}^{out} = 0, \quad \text{when } r = r_4 \quad (4.8)$$

4.4.2 Initial conditions

There is no stress in the three-layer cylinder at room temperature. So the temperature difference ΔT can be presented as

$$\Delta T = T(r) - T_0 \quad (4.9)$$

Where

$T(r)$ is temperature distribution in the three-layer cylinder.

T_0 is room temperature.

4.4.3 Continuity conditions

According to the structure integrity requirement, deformation must be continuous at the interphases, which means displacements at the interfaces (r_2 and r_3) are the same,

$$U^{in}(r) = U^{mid}(r), \quad \text{at } r = r_2 \quad (4.10)$$

$$U^{mid}(r) = U^{out}(r), \quad \text{at } r = r_3 \quad (4.11)$$

Where $U^{in}(r)$, $U^{mid}(r)$, $U^{out}(r)$ present the displacement distribution of the inner, middle and outer cylinders.

Since the three-layer cylinder is made of different materials and is exposed to a non-uniform temperature distribution, there must be pressure produced at the interfaces. Assume the expansion of the inner cylinder is bigger than that of the middle cylinder and the expansion of the middle cylinder is bigger than that of the outer cylinder, so there exist pressure at the interface r_2 and r_3 , which is p and p_1 respectively, see Figure 4.1, Figure 4.2, and Figure 4.3.

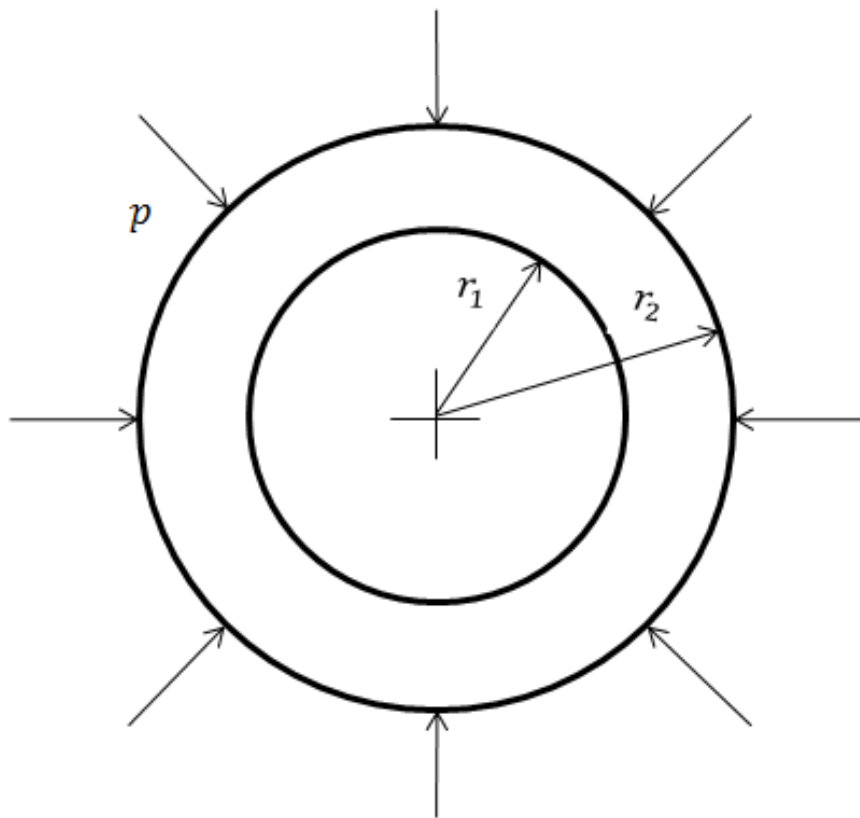


Figure 4.1 Pressure in the inner cylinder with inner radius r_1 and outer radius r_2

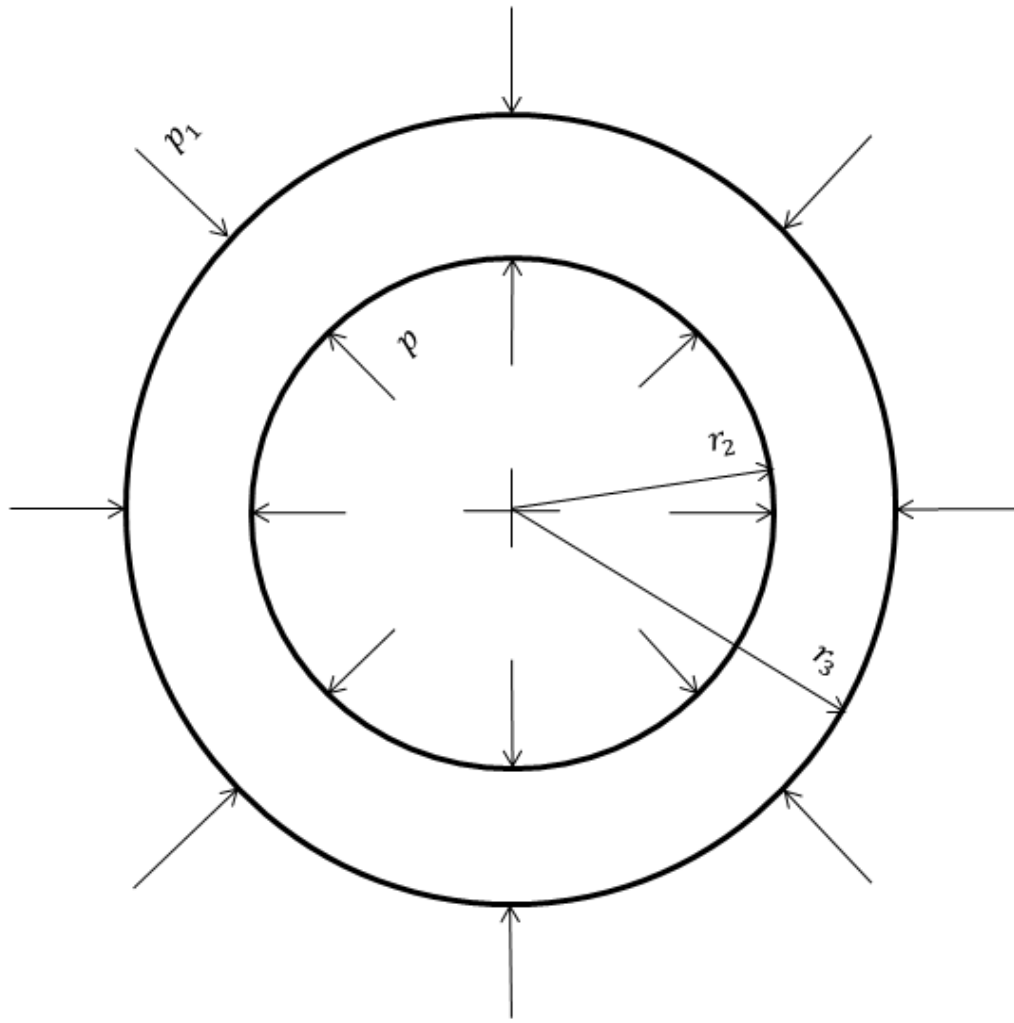


Figure 4.2 Pressure in the middle cylinder with inner radius r_2 and outer radius r_3

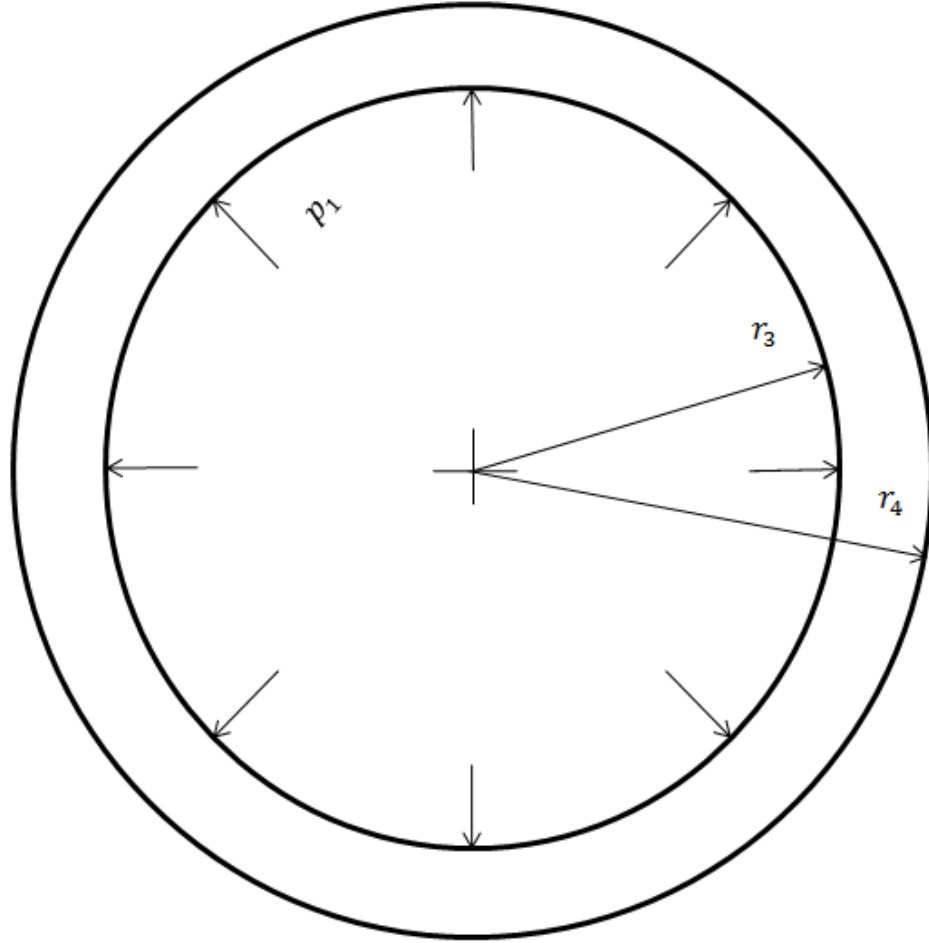


Figure 4.3 Pressure in the outer cylinder with inner radius r_3 and outer radius r_4

For the inner cylinder, at $r = r_2$, the unit outward normal is $\mathbf{n} = \mathbf{e}_r$ and the specified traction is $\mathbf{t} = -p$. It follows that

$$S_{rr}^{in} = -p, S_{\theta r}^{in} = 0, \text{ when } r = r_2 \quad (4.12)$$

For the middle cylinder, at $r = r_2$, the unit outward normal is $\mathbf{n} = -\mathbf{e}_r$ and the specified traction is $\mathbf{t} = p$. It follows that

$$S_{rr}^{mid} = -p, S_{\theta r}^{mid} = 0, \quad \text{when } r = r_2 \quad (4.13)$$

For the middle cylinder, at $r = r_3$, the unit outward normal is $\mathbf{n} = \mathbf{e}_r$ and the specified traction is $\mathbf{t} = -p_1$. It follows that

$$S_{rr}^{mid} = -p_1, S_{\theta r}^{mid} = 0, \quad \text{when } r = r_3 \quad (4.14)$$

For the outer cylinder, at $r = r_3$, the unit outward normal is $\mathbf{n} = -\mathbf{e}_r$ and the specified traction is $\mathbf{t} = p_1$. It follows that

$$S_{rr}^{out} = -p_1, S_{\theta r}^{out} = 0, \quad \text{when } r = r_3. \quad (4.15)$$

5.0 SOLUTIONS AND DISCUSSIONS

In the previous two chapters, heat transfer process in the particle bed and thermal stress analysis in the fuel element were illustrated respectively. The energy equation with auxiliary conditions in Chapter 3.0 contained sufficient information to solve temperature profile and the stress analysis of Chapter 4.0 also presented enough details to obtain the displacement and stress distributions. Based on the above, methods of determination of the temperature and thermal stress distributions were derived in this chapter. The effects of frits dimensions on thermal stress were also discussed.

5.1 SOLUTION TO ENERGY EQUATION

The energy equation (3.8) can be presented as follows,

$$-\frac{d^2T}{dr^2} + \left(\frac{\dot{m}C_{pf}}{2\pi k_s} - 1\right) \frac{1}{r} \frac{dT}{dr} + \frac{\dot{q}}{k_s} = 0, \quad r \in [r_2, r_3] \quad (5.1)$$

This is a second-order linear ordinary differential equation. Let

$$a = \frac{\dot{m}C_{pf}}{2\pi k_s} - 1, \quad b = \frac{\dot{q}}{k_s}. \quad (5.2)$$

The general solution for equation (5.1) is

$$T(r) = \frac{br^2}{2-2a} + \frac{C_1 r^{(a+1)}}{a+1} + C_2, \quad r \in [r_2, r_3] \quad (5.3)$$

where

C_1 and C_2 are constants to be determined.

With the auxiliary conditions,

$$C_1 = \frac{b(r_3^2 - r_2^2)}{(1-a)(r_2^{(1+a)} - r_3^{(1+a)})},$$

$$C_2 = T_1 - \frac{C_1 r_3^{(1+a)}}{1+a} - \frac{br_3^2}{2(1-a)}. \quad (5.4)$$

5.2 OUTLINE TO SOLVE DISPLACEMENT AND THERMAL STRESS

EQUATIONS

From former analysis, the temperature distribution in the three-layer cylinder can be got,

$$T(r) = \begin{cases} T_2, & r \in [r_1, r_2] \\ \frac{bx^2}{2-2a} + \frac{C_1 x^{(a+1)}}{a+1} + C_2, & r \in [r_2, r_3] \\ T_1, & r \in [r_3, r_4] \end{cases} \quad (5.5)$$

Using semi-inverse method, assume that the displacement field exhibits the same cylindrical symmetry as the boundary conditions, so that

$$u_r = U(r), \quad u_\theta = 0 \quad (5.6)$$

where $U(r)$ is a function that the governing equations and boundary conditions are satisfied.

It follows from the strain-displacement equation (4.1) that, if the displacement field is cylindrical symmetric, then the components of the strain field are given by

$$E_{rr} = U'(r), \quad E_{\theta\theta} = \frac{1}{r}U(r), \quad E_{r\theta} = 0 \quad (5.7)$$

So the constitutive equation (4.2) can be expressed as

$$\begin{aligned} S_{rr} &= (2\mu + \lambda) U'(r) + \lambda \frac{U(r)}{r} - (3\lambda + 2\mu)\alpha(\Delta T) \\ S_{\theta\theta} &= (2\mu + \lambda) \frac{U(r)}{r} + \lambda U'(r) - (3\lambda + 2\mu)\alpha(\Delta T) \end{aligned} \quad (5.8)$$

$$S_{zz} = \lambda \left(U'(r) + \frac{U(r)}{r} \right) - (3\lambda + 2\mu)\alpha(\Delta T)$$

And the equilibrium equation (4.3) becomes

$$\frac{\partial S_{rr}}{\partial r} + \frac{1}{r}(S_{rr} - S_{\theta\theta}) = 0 \quad (5.9)$$

Substituting constitutive equation (5.8) into equilibrium equation (5.9), it yields,

$$U''(r) + \frac{U'(r)}{r} - \frac{U(r)}{r^2} - \frac{(3\lambda + 2\mu)\alpha}{2\mu + \lambda}(\Delta T)' = 0 \quad (5.10)$$

where

$U'(r)$ and $U''(r)$ are the first and second derivative of $U(r)$ with respect to r .

$(\Delta T)'$ is the first derivative of ΔT with respect to r .

In the following part, the superscripts ⁱⁿ, ^{mid} and ^{out} represented the inner, middle, and outer cylinders, respectively. The subscripts ₁ and ₂ represented material 1 and material 2, respectively. It can be seen that Equation (5.10) is a second-order linear ordinary differential equation. Substituting the temperature distribution into it gives

$$\begin{aligned} U^{in}(r) &= A_1 r + \frac{B_1}{r}, \quad r \in [r_1, r_2] \\ U^{mid}(r) &= A_2 r + \frac{B_2}{r} + \frac{g \cdot r^{a+2}}{(a+1)(a+3)} + \frac{h \cdot r^3}{8}, \quad r \in [r_2, r_3] \end{aligned} \quad (5.11)$$

$$U^{out}(r) = A_3 r + \frac{B_3}{r}, \quad r \in [r_3, r_4]$$

where

$A_1, A_2, A_3, B_1, B_2, B_3$ are constants to be determined.

$$g = \frac{(3\lambda_2 + 2\mu_2) \cdot \alpha_2 \cdot C_1}{(2\mu_2 + \lambda_2)}, \quad h = \frac{(3\lambda_2 + 2\mu_2) \cdot \mu_2 \cdot b}{(2\mu_2 + \lambda_2)(1 - a)} \quad (5.12)$$

Substituting equation (5.11) to constitutive equations (5.8) gives

$$\begin{aligned} S_{rr}^{in} &= 2(\mu_1 + \lambda_1)A_1 - 2\mu_1 \frac{B_1}{r^2} - (3\lambda_1 + 2\mu_1) \cdot \alpha_1 \cdot (T_2 - T_0), \quad r \in [r_1, r_2]. \\ S_{rr}^{mid} &= 2(\mu_2 + \lambda_2)A_2 - 2\mu_2 \frac{B_2}{r^2} + r^2 \left[\frac{(2\lambda_2 + 3\mu_2) \cdot h}{4} - \frac{(3\lambda_2 + 2\mu_2) \cdot \alpha_2 \cdot b}{2 - 2a} \right] \\ &\quad + r^{m+1} \left\{ \frac{g[(a+2)(2\mu_2 + \lambda_2) + \lambda_2]}{(a+1)(a+3)} - \frac{(3\lambda_2 + 2\mu_2) \cdot \alpha_2 \cdot C_1}{a+1} \right\} \\ &\quad - (3\lambda_2 + 2\mu_2) \cdot \alpha_2 \cdot (C_2 - T_0), \quad r \in [r_2, r_3]. \end{aligned} \quad (5.13)$$

$$S_{rr}^{out} = 2(\mu_1 + \lambda_1)A_3 - 2\mu_1 \frac{B_3}{r^2} - (3\lambda_1 + 2\mu_1) \cdot \alpha_1 \cdot (T_1 - T_0), \quad r \in [r_3, r_4].$$

With the auxiliary condition in 4.4, there are eight equations (4.7), (4.8), (4.10)~(4.15) with eight unknowns ($A_1, A_2, A_3, B_1, B_2, B_3, p, p_1$), which are sufficient to get the exact solutions of displacement fields and stress fields in the three-layer cylinder.

5.3 RESULTS AND DISCUSSIONS

5.3.1 Temperature distribution

With given parameters' values in Chapter 2.3, temperature equation (5.1) is a function of mass flow rate \dot{m} and radius r , Figure 5.1 presents different temperature distributions with different

mass flow rates. To make sure the outlet temperature satisfies the requirement of the design which is 1000°C , the mass flow rate should be controlled at $0.5 \text{ kg}\cdot\text{s}^{-1}\cdot\text{m}^{-1}$, see Figure 5.2. This could be realized by controlling coolant velocity and pressure.

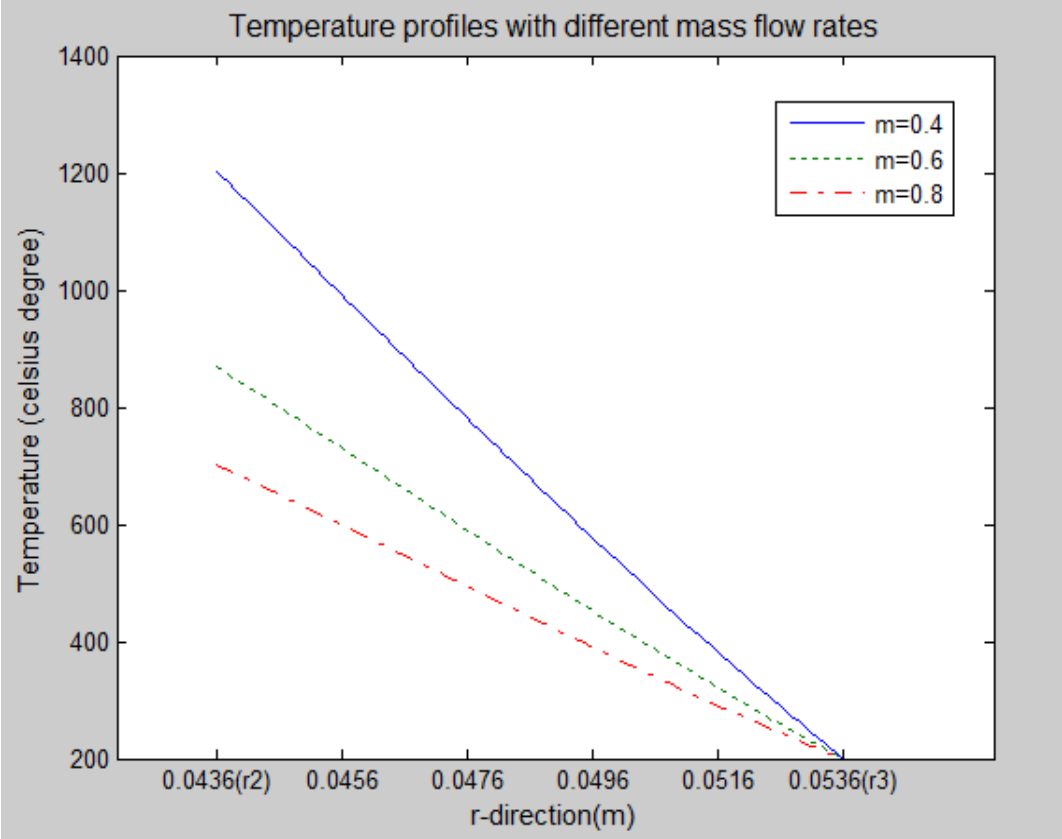


Figure 5.1 Temperature distributions in the middle cylinder with mass flow rate of 0.4, 0.6, and $0.8 \text{ kg}\cdot\text{s}^{-1}\cdot\text{m}^{-1}$, respectively.

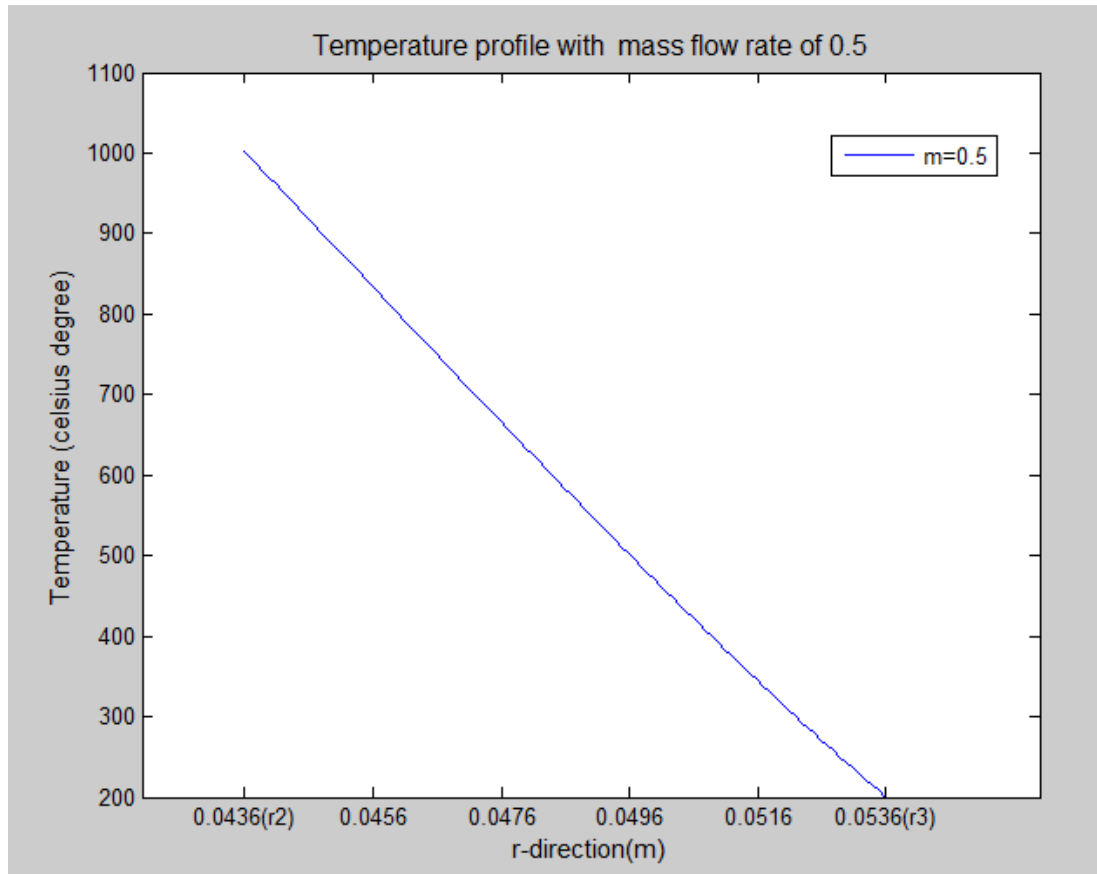


Figure 5.2 Temperature distribution in the middle cylinder with mass flow rate of $0.5 \text{ kg}\cdot\text{s}^{-1}\cdot\text{m}^{-1}$ and outlet temperature of 1000°C .

5.3.2 Displacement and thermal stress analysis

Figure 5.3~Figure 5.7 illustrate displacement and stress distributions in the three-layer cylinder based on frits thicknesses of 3mm ($r_1=0.0406$ m, $r_4=0.0566$ m).

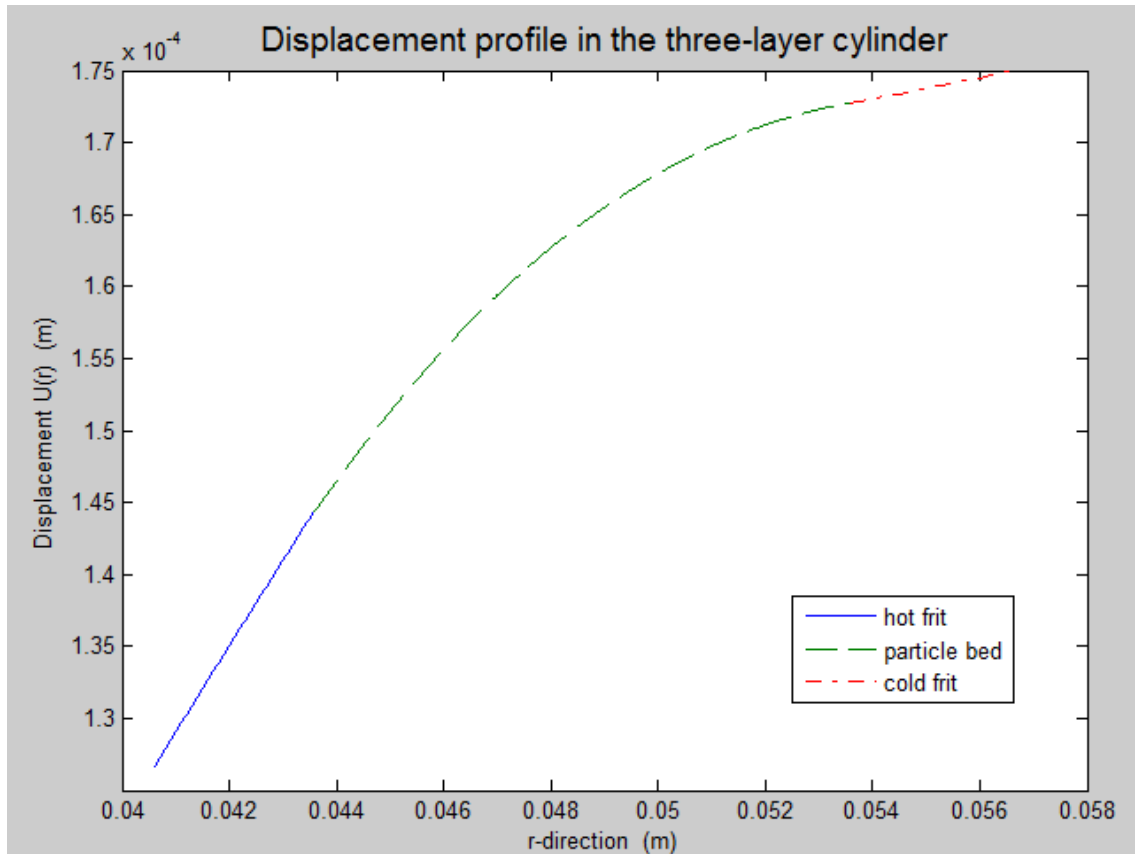


Figure 5.3 Displacement distribution in the three-layer cylinder with $r_1=0.0406$ m, $r_4=0.0566$ m.

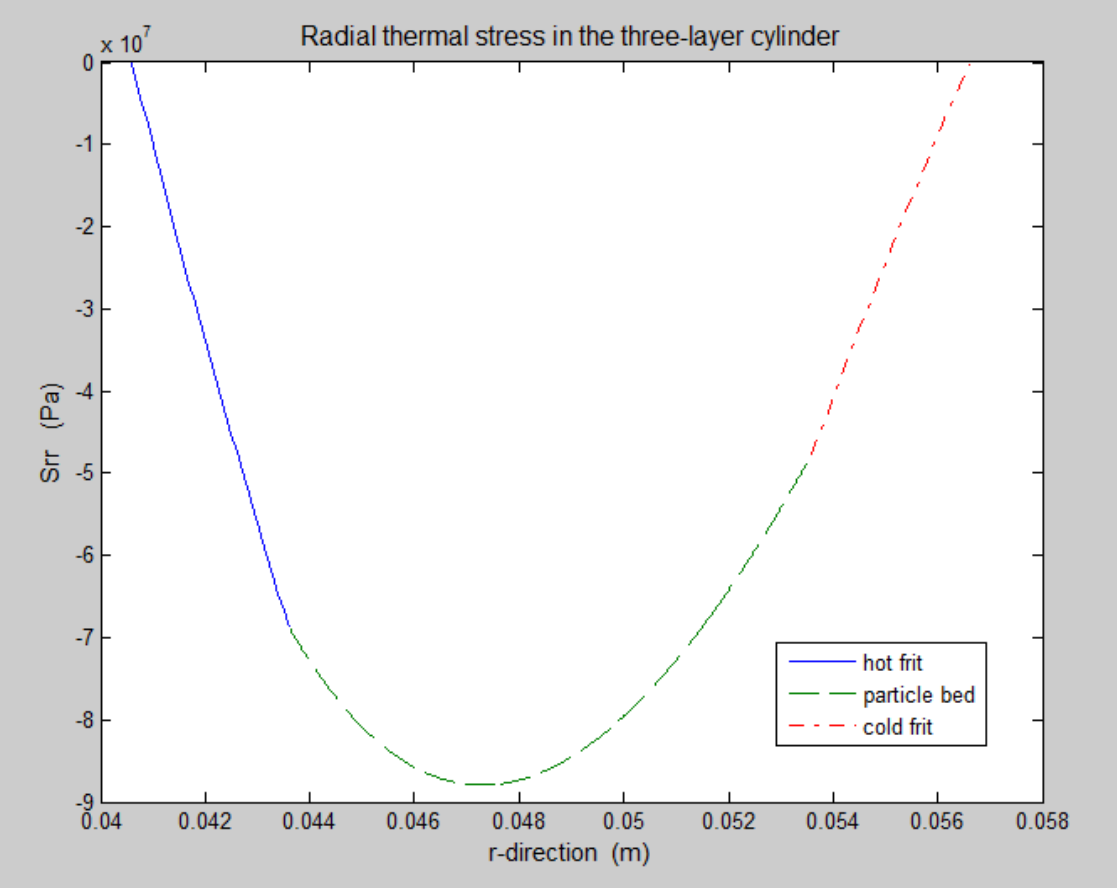


Figure 5.4 Radial thermal stress in the three-layer cylinder with $r_1=0.0406$ m, $r_4=0.0566$ m.

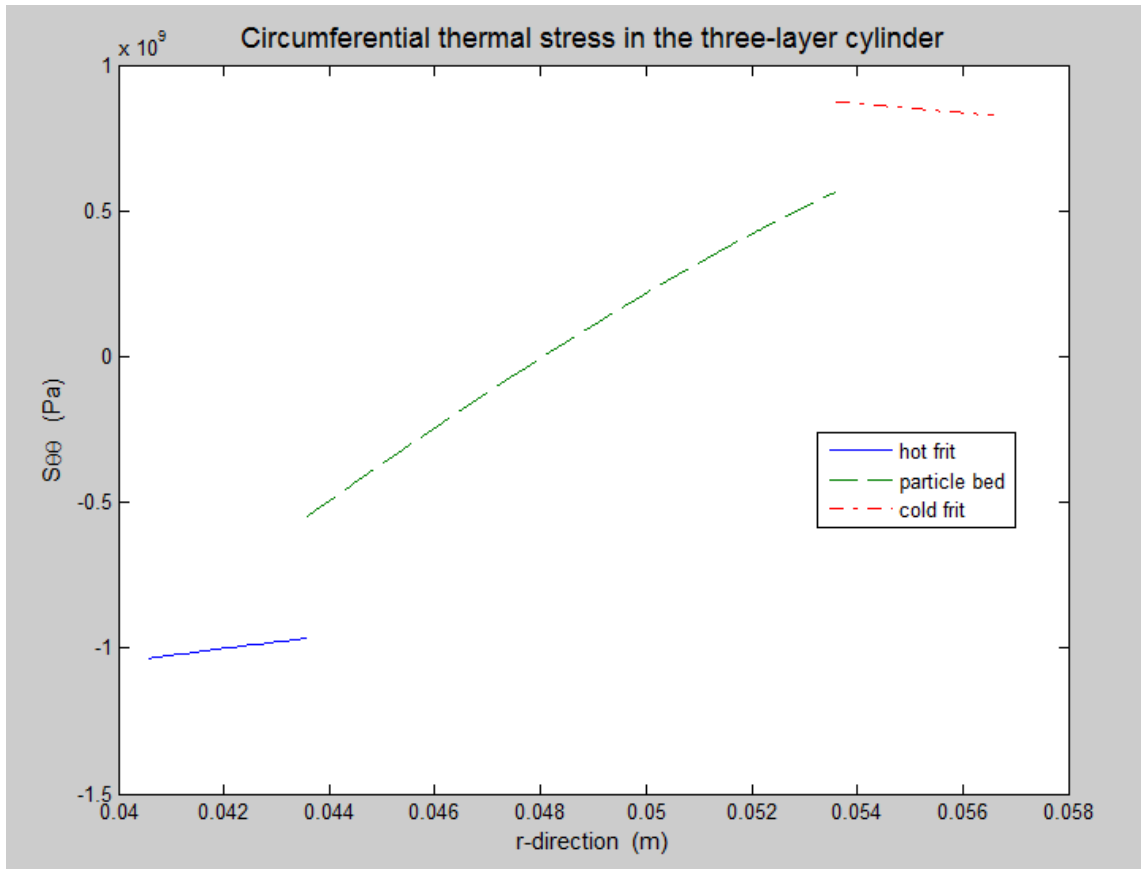


Figure 5.5 Circumferential stress in the three-layer cylinder with $r_1=0.0406$ m, $r_4=0.0566$ m.

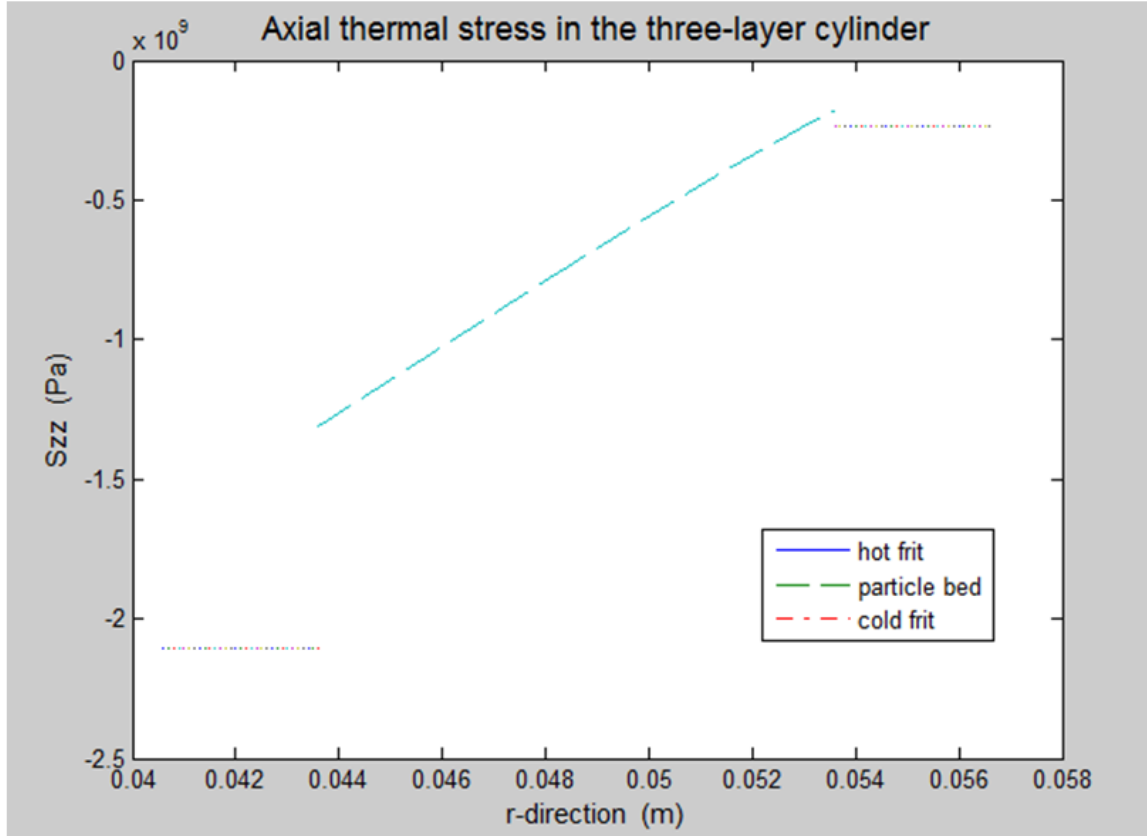


Figure 5.6 Axial stress in the three-layer cylinder with $r_1=0.0406$ m, $r_4=0.0566$ m.

Figure 5.3 shows the radial displacement in the three-layer cylinder and Figure 5.4-Figure 5.6 illustrate the stress distributions in three directions. The displacement by expansion in the three-layer cylinder is infinite small, but thermal stress produced by temperature gradient is extremely huge. The radial thermal stresses are continuous and compressive. However, tension appears in θ -direction and z -direction. The circumferential stress and axial stress have significant jumps at the interfaces as shown in Figure 5.5 and Figure 5.6. The discontinuity was due to the differences in the material properties such as Young's modulus and poisson's ratio. Linear thermal expansion coefficients of the two materials were assumed the same.

In the particle bed and cold frit, tension circumferential stress is not wanted for SiC is typically very brittle. It belongs to ceramic material which has excellent mechanical properties in

compression, but performs badly under tension. To keep the fuel particles in position, compressive stress in the particle bed was also preferred.

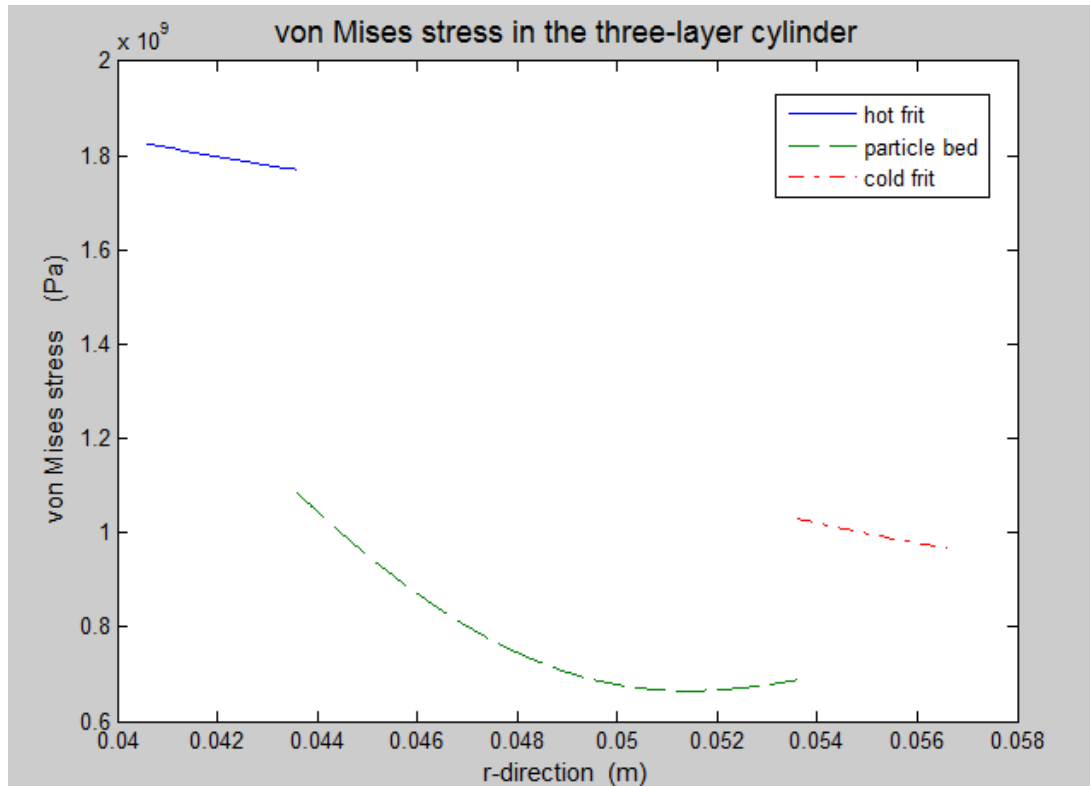


Figure 5.7 Von Mises stress in the three-layer cylinder with $r_i=0.0406$ m, $r_o=0.0566$ m.

Figure 5.7 illustrates yield stress by von Mises criteria [32] in the three-layer cylinder. As we expected, hot frit experiences the highest stress. Cracking is most likely to be initiated at the rim of the hot frit. Thus, more focus should be put on the hot frit design to make sure it accommodates the stress load and works without failure.

5.3.3 Geometry and thermal stresses

A summary of the effect of frits thickness on thermal stress was illustrated here. Just radial and circumferential stresses were presented. In plane strain state, the axial stress can be expressed in form of the other two stresses [33]. Since we didn't want particles redistribution in the particle bed, thermal stress in r -direction and θ -direction in the three-layer cylinder with different frit thickness were investigated.

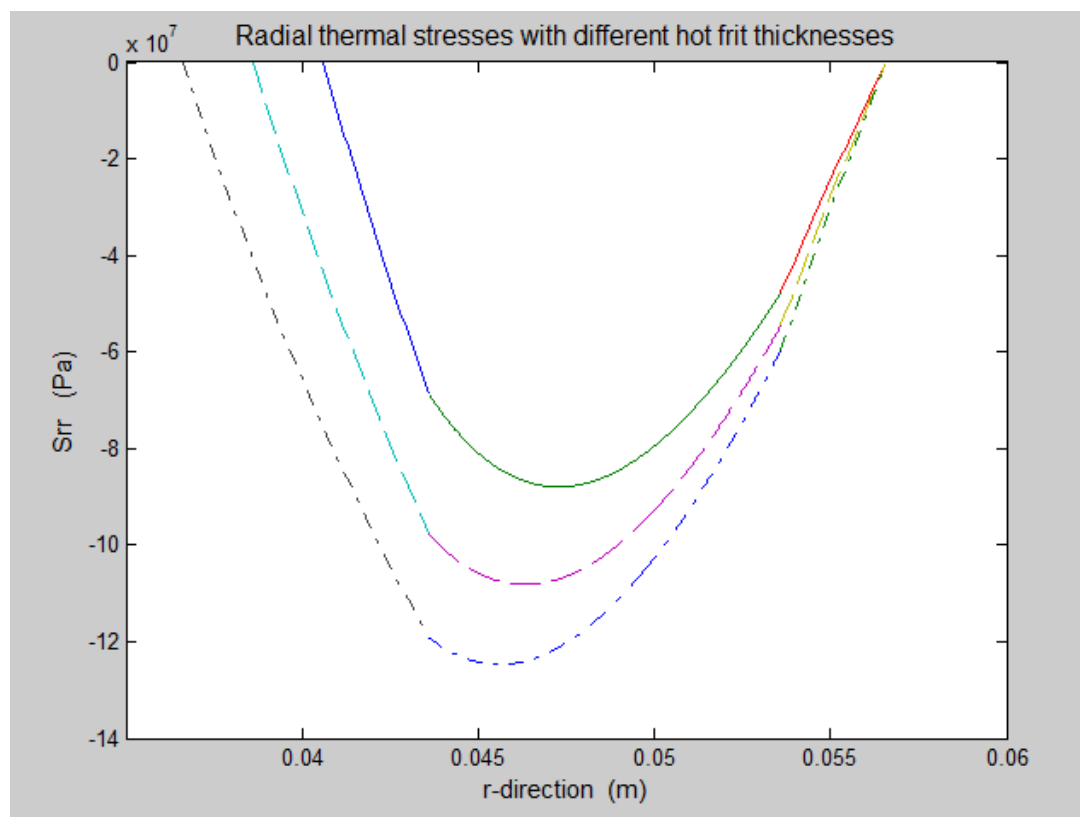


Figure 5.8 Radial thermal stresses in the three-layer cylinder with hot frit of 3mm ($r_f=0.0406m$), 5mm ($r_f=0.0386m$), and 7mm ($r_f=0.0366m$), respectively.

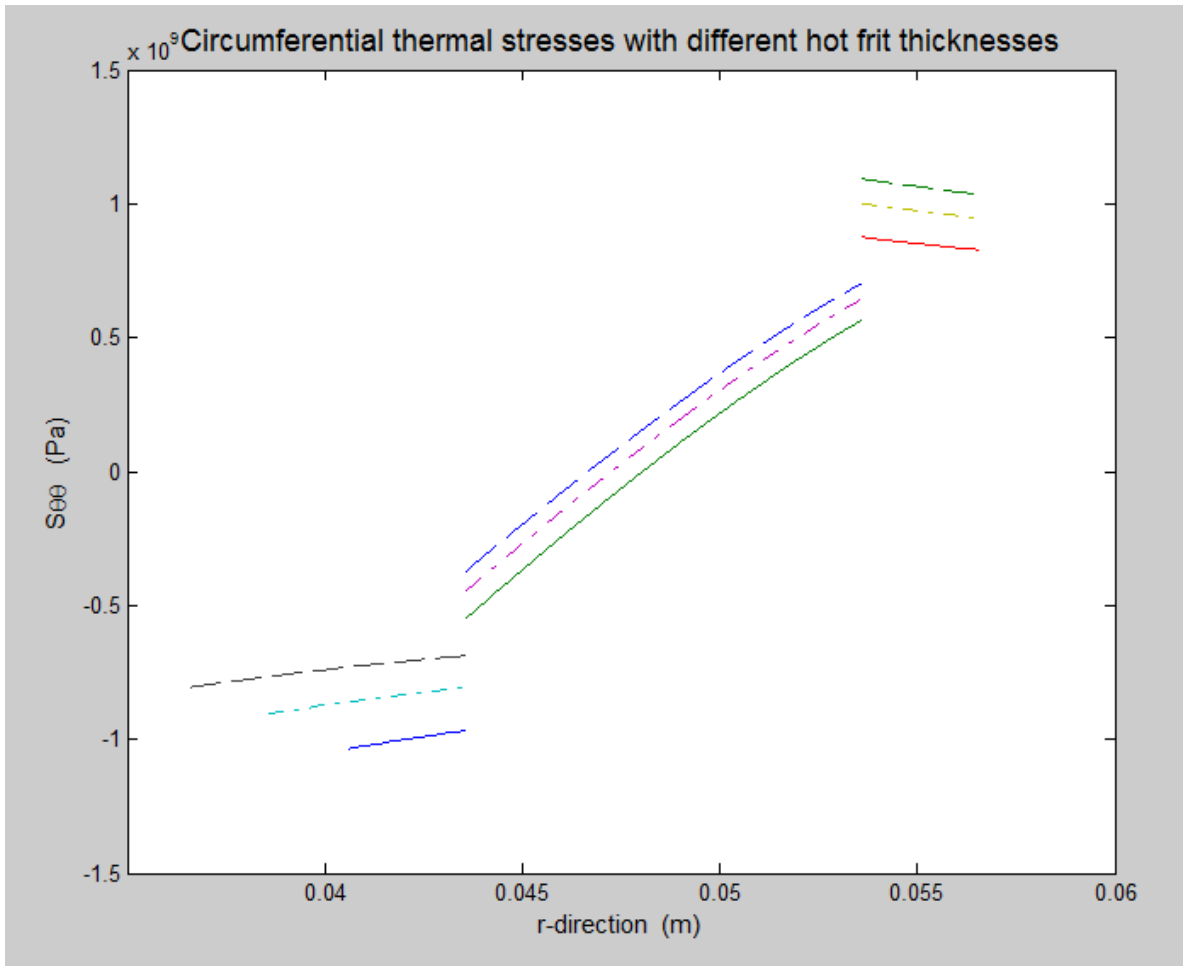


Figure 5.9 Circumferential thermal stresses in the three-layer cylinder with hot frit of 3mm ($r_I=0.0406$ m), 5mm ($r_I=0.0386$ m), and 7mm ($r_I=0.0366$ m), respectively.

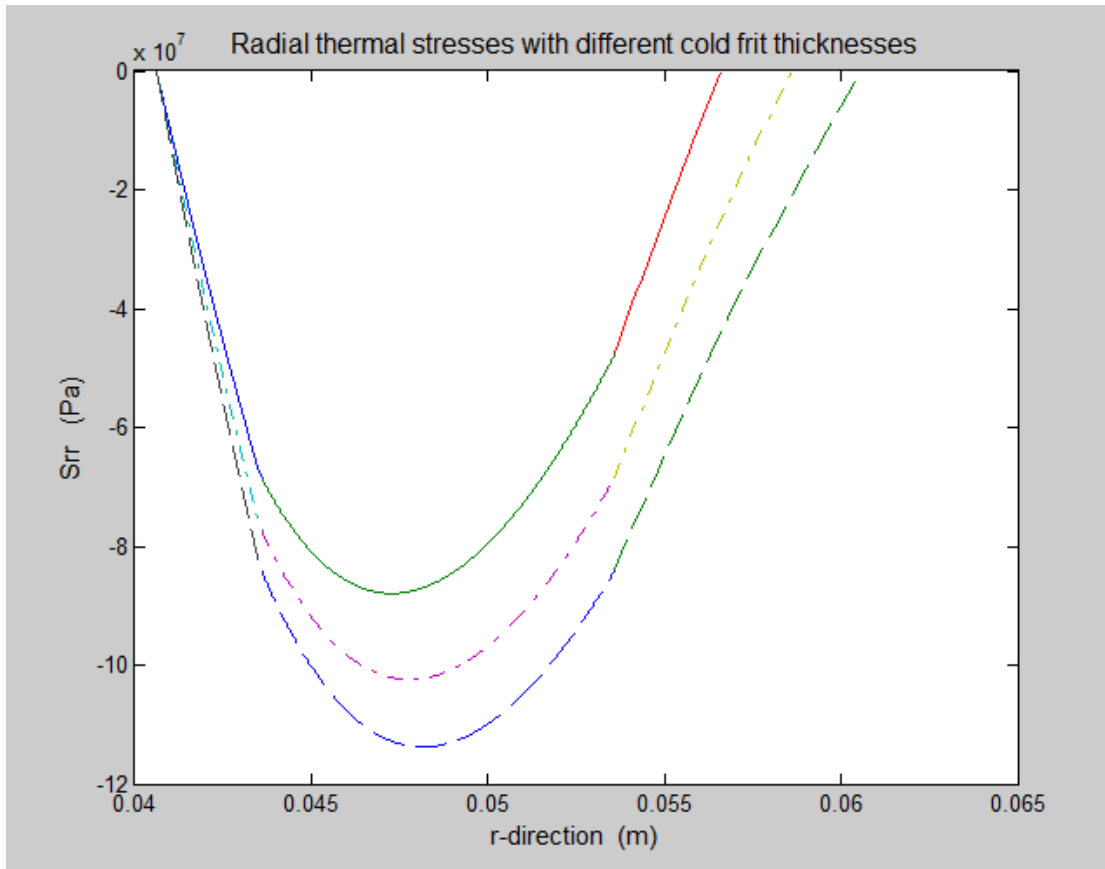


Figure 5.10 Radial thermal stresses in the three-layer cylinder with cold frit of 3mm ($r_4=0.0566$ m), 5mm ($r_4=0.0586$ m), and 7mm ($r_4=0.0606$ m), respectively.

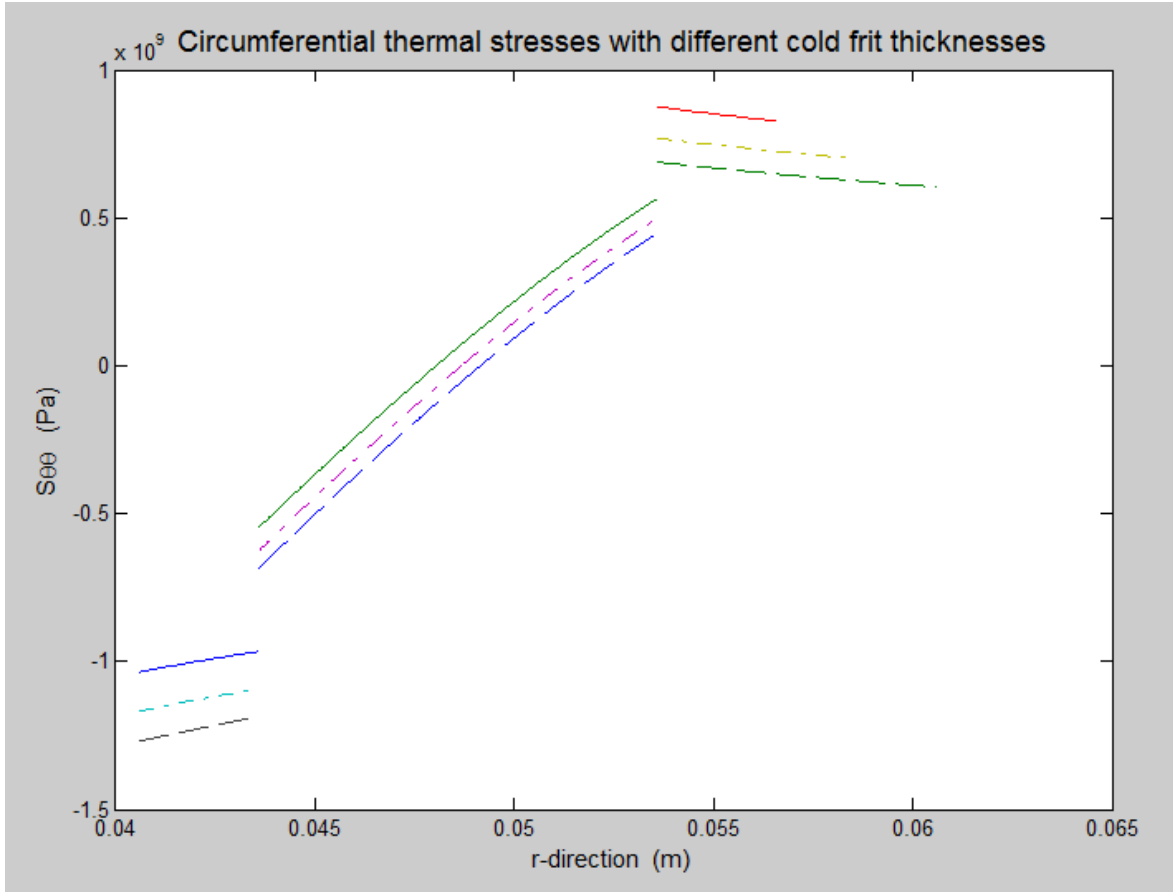


Figure 5.11 Circumferential thermal stresses in the three-layer cylinder with cold frit of 3mm ($r_4=0.0566\text{m}$), 5mm ($r_4=0.0586\text{m}$), and 7mm ($r_4=0.0606\text{m}$), respectively.

Figure 5.8 through Figure 5.9 illustrate how changing hot frit thickness affects thermal stress in r -direction and θ -direction. When the thickness of hot frit decreases, radial stress decreases. As to circumferential stress, when the thickness of hot frit decreases, tensile stress goes down. This is good for tensile stress is not wanted in the particle bed. It is not hard to understand for a thinner hot frit has a better compliance with the change.

The next group of figures, Figure 5.10 to Figure 5.11, illustrate how changing cold frit thickness affects thermal stress in r -direction and θ -direction. When the thickness of cold frit increases, radial thermal stress increases but tensile circumferential stress decreases. This is

because a thicker cold frit gives more confine on the whole structure. As we don't want tension exist in the particle bed and *SiC* performs better under compression, in the design limit, a thicker cold frit was preferred.

6.0 CONCLUSIONS

In this paper, a method of determination of temperature and thermal stress distributions in the fuel element was derived. To describe the fuel element, a three-layer porous cylinder with infinite height and different materials was considered. Heat transfer process was only considered in the particle bed. Temperatures of the frits were assumed to be constant. Numerical result of the temperature distribution in the particle bed was derived. In displacement and thermal stress analysis, the problem was taken as plane strain problem. The thermal and mechanical properties of the solid phase and coolant were taken as constants, which were independent of temperature and time. Some basic ideas were demonstrated in this study.

1. The steady state energy equation in a conductive porous medium with internal energy source in cylindrical coordinate was derived. The temperature of the solid phase and fluid phase are considered to be the same. The mechanical and thermal properties of solid and fluid phases are assumed to be constant.
2. Temperature distribution was obtained from the energy equation. It should be noted that different mass flow rate would lead to different temperature distribution with respect to r . To satisfy the requirement of the new design with an outlet temperature of 1000°C , the mass flow rate should be $0.5 \text{ kg}\cdot\text{s}^{-1}\cdot\text{m}^{-1}$ and this can be realized by controlling pressure and velocity of the coolant.

3. Displacement and thermal stress analyses in the three-layer cylinder were conducted based on presented temperature distribution. Thermal stress varied characteristically in each layer, especially for the occurrence of discontinuities at the interfaces. Radial thermal stress was compressive but tension appeared in circumferential stress in the particle bed and cold frit. Failure analysis was conducted based on von Mises criteria. It was shown that hot frit was most dangerous.
4. How changing thickness of frit affects thermal stress distribution was conducted. It was shown that within design requirement, a thinner hot frit and a thicker cold frit would give a better performance.

BIBLIOGRAPHY

1. Bruno, Claudio. *Nuclear Space Power and Propulsion Systems*. Reston, VA: American Institute of Aeronautics and Astronautics, 2008.
2. Metzger, John D., Enabling Technologies for a High Temperature, Gas-Cooled Particle Bed Reactor, Project draft for internal use, University of Pittsburgh, 2012.
3. Bussard, Robert W., and DeLauer Richard D. *Nuclear Rocket Propulsion* New York: McGraw-Hill, 1958.
4. Lawrence, T. J., Witter, J. K., and Humble, R. W. "Nuclear Rocket Propulsion Systems." in *Space Propulsion Analysis and Design*, ed. by Humble, R. W., Henry, G. N., and Larsen, W. J., New York: McGraw-Hill, 1995.
5. Turner, Martin J. L. "Nuclear propulsion." in *Rocket and Spacecraft Propulsion*, 219-269. Berlin: Springer-Praxis, 2005.
6. Gunn, Stanley "Nuclear Propulsion – a Historical Perspective." *Space Policy*, 17(2001): 291-298.
7. Dewar, J. A. *To the End of the Solar System: The Story of the Nuclear Rocket*, Lexington, KY: The Univ. Press of Kentucky, 2004.
8. Tuddenham, Read S. "Thermal Hydraulic Analysis of a Packed Bed Reactor Fuel Element." Master thesis, Massachusetts Institute of Technology, 1989.
9. Durham, F. P. "Nuclear Engine Definition Study Preliminary Report (Vol.1) – Engine Description", Los Alamos, NM: Los Alamos Scientific Laboratory Informal Report, 1972.
10. Koenig, Daniel R. *Experience Gained from the Space Nuclear Rocket Program (Rover)*. Los Alamos, NM: Los Alamos National Laboratory, 1986.
11. Hatch, L. P. et al., "Fluidized Beds for Rocket Propulsion", *Nucleonics*, 18 (1960):102.
12. Ludewing, Hans et al., "Feasibility of Rotating Fluidized Bed Reactor for Rocket Propulsion", *Journal of Spacecraft and Rockets*, 11(1974), pp. 65-71. doi: 10.2514/3.62010.

13. Ludewing, Hans et al., "Design of particle bed reactor for the space nuclear thermal propulsion." *Progress in Nuclear Energy*, 30 (1996): 1-65.
14. Powell, J. R. et al., "High Power Density Reactor Based on Direct-Particle Cooling", *Proc. Second Sym. in Space Nuclear Powell Systems*, Alb. NM., 1985.
15. Lazareth, O. W., et al., "Analysis of the Start-up and Control of a Particle Bed Reactor," *Space Nuclear Power System 1987*, ed. by M. S. El-Genk and M. D. Hoover, Malabar, FL: Orbit Book Co., 1988.
16. Horn, F. L., et al., "Particulate Fuel Bed Tests." *Space Nuclear Power Systems 1985*, ed. by M. S. El-Genk and M. D. Hoover, Malabar, FL: Orbit Book Co., 1986.
17. Lazareth, O. W., "Particle Bed Reactor Propulsion Vehicle Performance and Characteristics as an Orbital Transfer Rocket," *Space Nuclear Power Systems 1986*, ed. by M. S. El-Genk and M. D. Hoover, Malabar, FL: Orbit Book Co., 1987.
18. Vernon, M. E., "PIPE Series Experiment Plan." Sandia National Laboratory, Albuquerque, NM, 1988.
19. Haslett R. A., "Space Nuclear Thermal Propulsion Program Final Report." Grumman Aerospace Corporation, Bethpage, NY, 1995.
20. Power, J. R., and Horn, F. L., "High Power Density Reactors Based on Direct Cooled Particle Beds," *Space Nuclear Power System 1985*, ed. by El-Genk, M. S., and Hoover, M. D., Malabar, FL: Orbit Book Co., 1986.
21. Brinkley, Stuart. R., et al., "Heat transfer between fluid and porous solid generating heat." *J. Applied Physics*, 18 (1947): 582-585.
22. Choudhury, Wasi U. "Heat transfer and flow characteristics in conductive porous media with energy generation." Ph. D. Thesis, University of Wisconsin, 1968.
23. Marr, William W., "Hybrid computer solution of the energy equations in conductive porous media." Ph. D. Thesis, University of Wisconsin, 1969.
24. Green, D. W. and Perry, R. H. "Heat transfer with flowing fluid through porous media," *Chemical Engineering Progress Symposium Series*, No. 32, 57(1961): 61-68.
25. Leon Green. JR., and Downey, Calif., "Gas cooling of a porous heat source." *J. Applied Mechanics*, 1952: 173-178.
26. Holman, J. P. *Heat transfer*. Boston: McGraw Hill Higher Education, 2010.
27. Matthews, J. R., "Thermal stress in a finite heat generating cylinder." *Nuclear Engineering and Design*, 12 (1970): 291-296.

28. Valentin, Richard A., and Carey, John J., "Thermal stresses and displacements in finite, heat-generating circular cylinders." *Nuclear Engineering and Design*, 12 (1970): 277-290.
29. Orcan, Yusuf, "Thermal Stresses in a Heat Generating Elastic-Plastic Cylinder with Free Ends." *International Journal of Engineering Science*, 32 (1994): 883-898.
30. Lee, Z.Y., et al., "Transient thermal stress analysis of multilayered hollow cylinder." *Acta Mechanica*, 151 (2001):75-88.
31. Slaughter, William. S., *The Linearized Theory of Elasticity*. Boston: Birkhauser, 2002.
32. Ugural, Ansel C. and Fenster, Saul K., *Advanced Strength and Applied Elasticity*. Englewood Cliffs, N.J. : PTR Prentice Hall, 1995.
33. Timoshenko, Stephen P., and Goodier J. N., *Theory of Elasticity*. New York: McGraw-Hill, 1951.